UNIVERSIDADE DE LISBOA
FACULDADE DE CIÊNCIAS
DEPARTAMENTO DE FÍSICA

Development of motion compensated 3D T2 mapping for cardiac imaging

João Luís Silva Canaveira Tourais

Tese orientada por:

Prof. Dr. René Botnar, Division of Imaging Sciences & Biomedical Engineering, King's College London, United Kingdom
Dr. Rita Nunes, Instituto de Biofísica e Engenharia Biomédica, Departamento de Física da Faculdade de Ciências da Universidade de Lisboa, Portugal

MESTRADO INTEGRADO EM ENGENHARIA BIOMÉDICA E BIOFÍSICA
Perfil de Engenharia Clínica e Instrumentação Médica

DISSERTAÇÃO

2015

Resumo

A Ressonância Magnética Cardíaca (RMC) tem vindo a crescer tendo-se tornado numa excelente técnica de avaliação de doenças cardíacas, uma vez que produz imagens do coração de alta qualidade e de forma não ionizante. O edema do miocárdio é uma patologia em que ocorre aumento da quantidade de água o que se traduz num valor de T2 mais elevado nos tecidos. Para além do edema, outras patologias que levam a um aumento do valor do T2 são por exemplo o enfarte agudo do miocárdio, miocardite, tecidos transplantados rejeitados ou a sarcoidose. Por outro lado, valores de T2 mais baixos já foram encontrados em hemorragias no interior do miocárdio e em excessos crónicos de ferro em cardiomiopatias de ferritina. Esta relação faz com que o T2 e, portanto, as imagens ponderadas em T2 sejam bastante úteis em RMC.

No entanto, as imagens de RMC ponderadas em T2 normalmente apresentam limitações: são bastante sensíveis a movimentos dos órgãos, o sangue pode afetar o sinal medido nos tecidos e estas imagens estão sempre sujeitas a uma interpretação subjetiva por parte do médico. Assim sendo, recentemente foi proposta uma alternativa mais quantitativa, que foi denominada de mapeamento de T2. Normalmente, este método envolve a aquisição de três sequências T2prep, cada uma com diferentes tempos de eco do T2prep. O sinal em cada imagem representa um diferente tempo de eco ao longo da curva de decaimento em T2 e os mapas gerados são baseados nas três imagens com diferentes ponderações em T2.

Os mapeamentos de T2 podem fornecer uma deteção exata e confiável do tecido edematoso, presente no miocárdio, superando as limitações inerentes à análise de imagens ponderadas em T2. Contudo, as técnicas mais comuns de mapeamento de T2 ainda apresentam algumas limitações como a baixa resolução espacial e a incapacidade de corrigir corretamente o movimento, levando a que a maioria dos mapeamentos de T2 seja feita a duas-dimensões (2D) – ou seja apenas um corte – e em apneia. No entanto, apneias incompletas podem-se traduzir num mau co-registo das diferentes imagens, originando mapas incorretos. Na prática, longas aquisições e várias apneias são um entrave a mapeamentos de T2 de todo o coração – e não apenas só ao ventrículo esquerdo. Por exemplo, em situações onde o edema do miocárdio possa servir como um marcador de isquémia aguda (associada a dor torácica), certos pacientes têm dificuldade em tolerar múltiplas apneias e em permanecer longos tempos de aquisição dentro do magneto. Além disso, a maioria dos mapeamentos de T2 presentes na literatura foram testados e planeados para equipamentos de 1.5T.

Paralelamente, têm sido utilizadas algumas técnicas para limitar o efeito do movimento respiratório durante as aquisições das imagens – denominadas de navegadores.

O navegador diafragmático a uma-dimensão (d1D NAV) – também denominado por *pencil beam* – é a abordagem mais simples e baseia-se numa relação linear entre o diafragma e o movimento respiratório. No entanto, para além do planeamento que é necessário antes da aquisição das imagens – de modo a colocar o navegador perto do diafragma – é também difícil de prever o tempo extra que esta abordagem vai implicar, uma vez que esta técnica é pouco eficiente para ciclos respiratórios e cardíacos irregulares. Estas limitações levaram a que um tipo de navegador diferente fosse criado, ao qual se chamou auto-navegação. Com esta abordagem o movimento respiratório é calculado diretamente a partir dos dados, removendo a necessidade de um modelo de movimento do diafragma. No entanto, esta técnica pode incluir na estimativa do movimento dos pulmões alguns tecidos estáticos (como por exemplo a parede torácica), o que pode levar a uma incorreta estimativa do movimento. Muito recentemente, uma nova técnica foi proposta – e foi utilizada neste trabalho incorporada na sequência utilizada para obter os mapeamentos de T2 – chamada de navegação baseada em imagem (iNAV).

Com o iNAV, antes da aquisição principal, são obtidas imagens do coração de baixa resolução. Estas imagens de baixa resolução são utilizadas para automaticamente e em tempo real, calcular o movimento do coração. Este cálculo do movimento do coração, é feito através de um algoritmo – adaptado de uma versão previamente existente – que utiliza a informação das imagens de baixa resolução e separa os tecidos em movimento dos tecidos estáticos levando a uma estimativa precisa do movimento respiratório.

O trabalho aqui apresentado consistiu no desenvolvimento, teste e validação de uma nova abordagem para o mapeamento de T2 que permite a aquisição de um volume a três-dimensões (3D) cobrindo assim todo o coração. A esta abordagem, foi englobado o iNAV, que reduz drasticamente o tempo de aquisição, permitindo que o sujeito possa respirar livremente durante a realização do exame. Sendo a sua eficiência de 100% é possível prever o tempo esperado para o exame. Apesar de outros navegadores (como por exemplo o *pencil beam* e a auto-navegação) já terem sido utilizados para melhorar o mapeamento de T2, não existem estudos que tenham recorrido ao iNAV.

É de realçar ainda o facto de se usar um impulso de saturação, fazendo com que esta abordagem seja insensível a variações na frequência cardíaca e permitindo que sejam adquiridas imagens em todos os batimentos cardíacos, não sendo necessário esperar muito tempo para recuperar a magnetização T1. Outra das vantagens da sequência apresentada é o facto de as imagens se encontrarem espacialmente alinhadas usando volumes intercalados com diferentes ponderações em T2. As aquisições a 3D melhoram quer a compensação do movimento através dos vários planos quer a razão sinal-ruído (RSR) em comparação com técnicas anteriores.

A precisão desta técnica foi medida usando fantomas de gel com diferentes valores de T1 e T2 e foi demonstrada em aquisições a 3D para mapeamento de T2 do coração em humanos saudáveis (isto é, sem nenhuma patologia cardíaca) num equipamento de 3T. Para se proceder à validação desta abordagem foram comparados os resultados dos mapeamentos de T2 utilizando a correção do movimento feita

pelo iNAV e através do *pencil beam*. Finalmente, foi feita a análise estatística para comparar os resultados obtidos.

Os mapeamentos de T2 a 3D revelaram resultados consistentes com os métodos mais tradicionais no caso dos voluntários analisados. O valor de T2 obtido para o miocárdio foi de 45.7 $\pm$ 5.7 ms utilizando a técnica desenvolvida neste trabalho (tempo de aquisição = 4.56 $\pm$ 1.7 min), 47.1 $\pm$ 8.9 ms utilizando a correção feita pelo *pencil beam* (tempo de scan = 14.2 $\pm$ 3 min) e 46.1 $\pm$ 6.3 ms numa aquisição a 2D e em apneia. Após a análise estatística, conclui-se que os valores de T2 não apresentam diferenças significativas entre métodos ($p < 0.05$).

A técnica desenvolvida neste trabalho permite obter mapeamentos de T2 a 3D do coração de forma precisa e em menos de 5 minutos. Além disso, esta abordagem permite que o paciente respire livremente aquando da aquisição das imagens e apresenta resultados similares aos que se obtêm com a abordagem a duas dimensões. Apesar de não ter sido possível testar a técnica proposta em pacientes, acredita-se que é possível utiliza-la sem qualquer restrição. Trabalhos futuros podem incluir o teste deste método na caracterização de diferentes patologias cardíacas, bem como na tentativa de combinar a técnica aqui proposta com métodos de aquisição paralela, que permitam reduzir ainda mais o tempo de scan. É possível concluir que os objetivos foram atingidos e os resultados bastante promissores nesta abordagem inovadora, uma vez que não há registos de mapeamentos de T2 juntamente com o iNAV.

Palavras-chave: Ressonância Magnética Cardíaca; Mapeamento de T2; Respiração livre; Correção de movimento respiratório; iNAV.

Abstract

Purpose: T2 mapping can detect variations in the water content of the myocardium. As it consists of a quantitative approach, this technique overcame some of the limitations present in the commonly used T2-weighted MRI. In fact, this type of methodology is becoming increasingly important for tissue characterization in patients with myocardial pathologies (e.g. myocardial edema). As a large set of images may be needed to calculate each parameter, scans have been typically limited to 2D images acquired during breath-holding (BH). The aim of this project was to extend the commonly used breath hold approaches enabling free breathing while attaining high resolution whole heart images by developing and test a free-breathing, whole heart T2 mapping technique at 3.0T.

Methods: To generate T2 maps, multiple images are acquired with varying degrees of T2 weighting using magnetization preparation. In this work, image-based navigation (iNAV) was combined with a dynamic T2 prepared sequence with a varying T2prep echo time to investigate the feasibility of iNAV for T2 mapping with 100% scan efficiency. ECG-triggering, interleaved acquisitions and a saturation pulse – to reset the magnetization on every heartbeat – were used in the module. A monoexponential function is adjusted to the images intensities and with the fitting the T2 maps are generated. The work consisted in adapting the MRI pulse sequence for T2 mapping by introducing iNAV for respiratory motion correction and evaluation of the new 3D T2mapping scan in phantoms as well as healthy subjects.

Results: In healthy volunteers the T2 values did not display significant differences ($p < 0.05$) when the results obtained with the proposed approach (45.7 ± 5.7 ms), were compared to those obtained with previous methods - the 3D T2prep corrected with the pencil beam navigator (47.1 ± 8.9 ms) and the breath-held 2D T2prep (46.1 ± 6.3 ms).

Conclusion: The proposed free-breathing whole heart 3D T2 mapping approach is feasible and can be performed within less than 5 min with similar accuracy to that of the 2D-BH T2 mapping approach. Also, it may be applicable in myocardial assessment instead of current clinical black blood sequences.

Keywords: Cardiac Magnetic Resonance Imaging; T2 mapping; Free breathing; Respiratory motion correction; Image-based navigator.

Acknowledgements

During my academic journey and in particular in the six months spent in London, several people have been by my side showing their support and believing in my abilities. This particular work would not have been possible without the dedication and endeavor of all people who were involved in it. It was a privilege to spend these six months in the Division of Imaging Sciences & Biomedical Engineering at King's College London, surrounded by amazing people. I would like to write a few lines to show my gratitude.

First of all, I am thankful for my supervisor, Professor **René Botnar**, receiving me in the King's College London. He provided the vision, the motivation and the best advice that I could ever have had. Professor **René Botnar** supported me throughout this mission, sharing his knowledge and providing all the help I have needed. He greatly contributed for my education and showed me what doing research abroad is all about. For me it was an honour to have worked with him.

I would like to express my deepest gratitude to Dr **Markus Henningsson** for all the patience, hard working days, useful corrections, and for being always there when I needed. His involvement in this project made it possible to achieve a great work and more important, for me to have fun, whilst doing something I like. I am indebted to him for guiding me on a daily basis. I appreciate all his contributions of time and all the energy that he focuses on my work.

I would like to thank to Dr **Rita Nunes**, my internal supervisor, for all the support during this project, all the motivation and all the encouragement in this amazing experience. As my supervisor, her regular and prompt feedback and optimism were crucial for this work. Without her, this work would not have been successful at all. I would like to show my appreciation for Dr **Rita Nunes** being always available to help me and, most of all for all the support and encouragement that she provided during the five years that I have been a student in the Faculty of Sciences. Dr **Rita Nunes** was always the kind of teacher that believed in her students and, therefore, she is an inspiration as a person. I hope to sustain her example in my future pursuits.

I would also like to thank to rest of our group (**Alkystis**, **Andrea**, **Arna**, **Bego**, **Dirk**, **Isabel**, **Maryam**, **Melissa** and **Sara**) for all the help, support and advices. They were always there for me, and without their help the work would have been much more difficult. I say to them a very thoughtful thank you for making my stay in London one of the best experiences of my life. My sincere thank you for making me feel at home and it was a pleasure to meet you, inside and outside the walls of the office.

I gratefully acknowledge financial support from the Erasmus student interchange Grant.

I am also grateful for the friends I met in the University, because they have been by my side in my down moments, but even better because we celebrated together our achievements. To all my friends at FCUL many thanks for all the pleasurable moments. I leave a special word to **Francisco**, **Célia** and **Nádia**, who shared this London experience with me.

If there was someone who encouraged me to endeavor such an adventure was my girlfriend, **Filipa Guerreiro**. Not only she helped me whenever I needed but she was also a major source of unconditional support in the good but also in the bad moments. All the words are not enough to thank all the company, the support and all the encouragement.
Thank you for being a source of strength and inspiration. Thank you for all the love and affection. Without you by my side, I would never get this far.

Lastly, but the most important acknowledgment, I thank my **parents**, my **brother** and the rest of my family for providing all the conditions for my success while a student. Because they were and they will always be present for me. Thank you for all the financial and emotional support, motivation, and for always believing in me. Anything of this would have been possible without you.

Contents

List of Abbreviations

BB Black-blood

BOLD Blood oxygenation level-dependent

BH Breath-hold

CMR Cardiac Magnetic Resonance

COV Coefficient of variation

CT Computed Tomography

d1D NAV Diaphragmatic one-dimension navigator

ECG Electrocardiography

ECV Extracellular volume

FOV Field-Of-View

FH Foot-head

FID Free induction decay

GraSE Gradient spin-echo

iNAV Image-based navigation

KWIC K-space weighted image contrast

LGE Late Gadolinium Enhancement

LV Left ventricle

LR Left-right

MRI Magnetic resonance imaging

MI Myocardial infarction

PB Pencil Beam

RF Radiofrequency

ROI Region of interest

RV Right ventricle

SAT Saturation

SAX Short-axis

SNR Signal-to-noise ratio

SPGR Spoiled gradient echo

SSFP Steady-state free-precession

T1W T1-weighted

T2prep T2-preparation

T2W T2-Weighted

3D Three-dimensional

TE Time of echo

TR Time of Repetition

2D Two-dimensional

2DSN Two-dimensional self-navigator

List of Tables

List of Figures

Chapter 1

Introduction

Cardiac magnetic resonance (CMR) imaging is a well-established noninvasive imaging modality in clinical cardiology. CMR due to its capacity of defining cardiac morphology accurately and to investigate the function of the cardiac tissues has become one of the most used techniques in clinical routine. The introduction of Late Gadolinium Enhancement (LGE) led to an improvement in CMR regarding tissue characterization, once this technique made it possible to differentiate ischemic heart disease from nonischemic cardiomyopathies [1]. However, analysis of these images still presents some difficulties in the identification of areas of edema and inflammation when present in the myocardium [2]. To address this, quantitative measurements of the myocardial tissues have been proposed [3].

These quantitative techniques are commonly known as T1 or T2 mapping – depending on the ponderation of the acquired images. These novel mapping strategies allow an absolute quantitative measure instead of a visual (qualitative) analysis, which removes the subjectivity and the under- or overestimation in case of diseased tissues.

T2 mapping is accomplished by acquiring various images with different T2-weighting (T2W), providing multiple points along the T2 decay curve for fitting an exponential signal decay model [3]. The first approaches for T2 mapping relied on dark-blood turbo spin echo sequences, but this technique was very sensitive to ghosting and motion artifacts [3]. In the last 5 years different techniques have been proposed and tested, based on bright-blood T2 prep-based pulse sequences [4]. However, some limitations related with heart-rate dependency, incomplete T1 recovery, inter-individual variability or low SNR of the images still remained [5]. In order to address these problems, the proposed technique was constructed in a way to minimize their influence. The strategies include the introduction of a saturation pulse right after the QRS segment of the ECG, the possibility of interleaving acquisitions and the use of a 3T scanner – the majority of the previous studies were done at 1.5T.

Also the majority of the T2 mapping methods presented in the literature require a breath-hold acquisition scheme and do not usually cover the whole-heart. The proposed technique permits the acquisition of a 3D volume and allows the subject to breath freely during the whole scan. By allowing free breathing during the acquisitions, it becomes necessary to correct for the motion of the heart and the lungs. The effects of heart motion are minimized using the ECG during the scanning procedure

and gating the image acquisition so that it is performed during diastole – when the myocardium is not moving. Regarding the respiratory motion, several approaches have been proposed.

A diaphragmatic 1D navigator is normally used to correct for the respiratory motion in CMR scans [6]. With this approach, a constant linear relationship is assumed between diaphragmatic and cardiac respiratory motion. However, these assumptions result in some limitations and require more scan planning time. These limitations have motivated a different respiratory motion compensation approach, called self-navigation [7]. With this approach, motion can be estimated directly from the data, removing the necessity of a diaphragmatic motion model [8]. However, some static tissue (like the chest wall) may contribute to the navigator, affecting its motion estimation performance. More recently, a technique called image-based navigation (iNAV) [9] has been proposed, and it was used in this work to obtain the T2 maps.

With this method the images are corrected in real-time, using a very low resolution image acquired on every heart-beat and prior to the main MR acquisition. With this low-resolution image, the movement of the heart can be easily separated from the static tissues, leading to an improvement in the respiratory motion estimation [9].

With the combination of this novel technique for motion correction, the duration of the scan for T2 mapping is expected to be shorter compared to other studies presented in the literature, once there are no records of T2prep-based cardiac T2 mapping approaches combined with iNAV. This project consisted in the development and testing of the T2 mapping sequence module in phantoms and in healthy human volunteers to assess the accuracy and robustness of the proposed approach.

1.1 Objectives

The main goals of this project were:

- Implement a dynamic T2 prepared sequence with changeable T2prep echo time and segmented k-space acquisition to enable high resolution 3D T2 mapping.
- Include iNAVS for respiratory motion correction of 3D T2 mapping with multiple independent image navigators.
- Evaluate the performance of the T2 mapping in phantoms with known T2 values.
- Test the performance and the accuracy of the T2 mapping in healthy subjects.

1.2 Outline

This thesis comprises 6 chapters. In each chapter, the information considered to be relevant for the understanding of the proposed motion compensated 3D T2 mapping for cardiac imaging is presented.

In the next chapter, a background overview is addressed, including significant concepts of T2 mapping, respiratory navigators and also the state-of-the-art of cardiac T2 mapping. In Chapter 3, the pulse sequence composition is explained and the

methods and materials used to test it are described. The results from the developed work are presented in Chapter 4, whereas the results are discussed in Chapter 5. Finally, Chapter 6 summarizes the results and final conclusions of this research and presents suggestions for future work.

Chapter 2

Background

2.1 Magnetic Resonance

Atoms with an odd number of protons and/or odd number of neutrons possess a nuclear spin angular momentum, and therefore exhibit the magnetic resonance (MR) phenomenon. The protons and neutrons of the nucleus have a magnetic field associated with their nuclear spin. Associated to the proton nucleus is also their charge distribution. Resonance is an energy coupling that causes the individual nuclei, when placed in a strong external magnetic field, to be able to selectively absorb, and later release, energy unique to those nuclei and their surrounding environment – i.e. the frequency is a particular characteristic of each nucleus. Qualitatively, these nucleons can be visualized as spinning charged spheres that give rise to a small magnetic moment.

In biological specimens, hydrogen ^{1}H, with a single proton, is the most abundant atom (the body consists largely of H_2O – water – and fat) and the most sensitive (that is, it gives rise to the largest signals). Because of the abundance of the hydrogen nucleus, its nuclear MR signal can be used to generate an image. Magnetic resonance imaging (MRI) depends on the existence of the inherent angular momentum, or spin, of protons (^{1}H) and neutrons that is a basic property of matter. Hydrogen nuclei, composed of protons, have spin and interact with magnetic fields. In the absence of a magnetic field, the hydrogen spins are randomly oriented. However, if placed in a strong magnetic field (called B_0), the fat and water spins (i.e., the ^{1}H nuclear magnets) partly align with this applied magnetic field. This is why the hydrogen nuclei in MRI are also referred to as spins: they spin, or precess, around the B_0 field [10].

MRI is a rapidly changing and growing imaging modality. The high contrast sensitivity to soft tissue differences and the inherent safety for the patient resulting from the use of nonionizing radiation have been key reasons why MRI has supplanted many Computed Tomography (CT) and projection radiography methods. With continuous improvements in image quality, acquisition methods, and equipment design, MRI is the modality of choice to examine anatomic and physiologic properties of the patient. There are drawbacks, including high equipment and setting up costs, scan acquisition complexity, relatively long imaging times, significant image artifacts, and patient claustrophobia problems [10].

2.2 Free Induction Decay: T2 Relaxation

Application of radiofrequency (RF) energy synchronized to the precessional frequency of the protons causes displacement of the tissue magnetic moment from equilibrium conditions (i.e., more protons are in the antiparallel orientation). Return to equilibrium results in emission of MR signals proportional to the number of excited protons in the sample, with a rate that depends on the characteristics of the tissues. Excitation, detection, and acquisition of the signals constitute the basic information necessary for MRI [10]. Also it can be said that the application of RF modifies the orientation of magnetization allowing it to be brought to the transverse plane.

A 90°RF pulse produces phase coherence of the individual protons and generates the maximum possible transverse magnetization (M_{xy}) for a given sample volume. As M_{xy} rotates at the Larmor frequency – the precession angular velocity – the receiver antenna coil is induced (by magnetic induction) to produce a damped sinusoidal electronic signal known as the free induction decay (FID) signal (Figure 2.1).

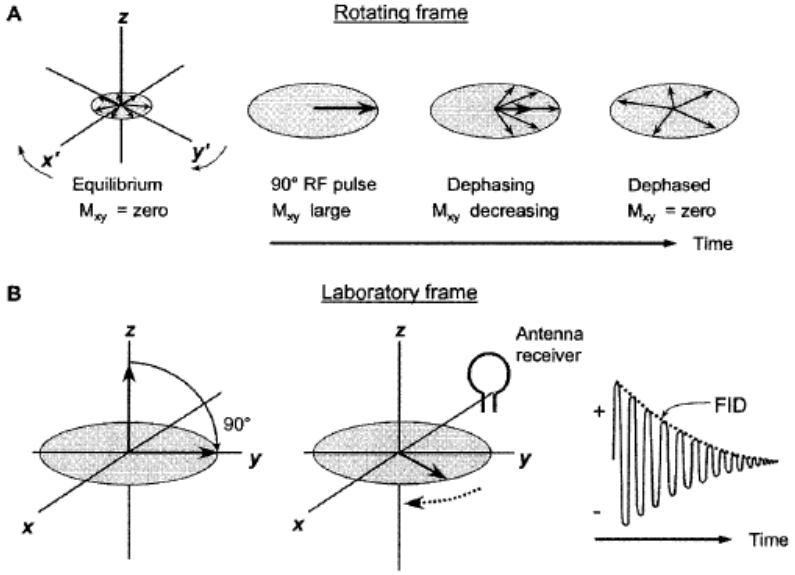

Figure 2.1: A: Conversion of longitudinal magnetization, M_z, into transverse magnetization, M_{xy}, results in an initial coherence of the phase of the individual spins of the sample. The magnetic moment vector precesses at the Larmor frequency (stationary in the rotating frame) and dephases with time. B: In the laboratory frame, M_{xy} precesses and induces a signal in an antenna receiver that is sensitive to transverse magnetization. A free induction decay (FID) signal is produced, oscillating at the Larmor frequency, and decays with time due to the loss of phase coherence. Adapted from [10].

The "decay" of the FID envelope is the result of the loss of phase coherence of the individual spins caused by magnetic field variations. Micromagnetic inhomogeneities intrinsic to the structure of the sample cause a spin-spin interaction, whereby the individual spins precess at different frequencies due to slight changes in the local magnetic field strength. Some spins precess faster and some slower, resulting in a loss of phase coherence. External magnetic field inhomogeneities arising from imperfections in the magnet or disruptions in the field by paramagnetic or

ferro-magnetic materials accelerate the dephasing process. Exponential relaxation decay, T2, represents the intrinsic spin-spin interactions that cause loss of phase coherence due to the intrinsic magnetic properties of the sample. The elapsed time between the peak transverse signal and 37% of the peak level $1/e$ is the T2 decay constant (Figure 2.2). Mathematically, this exponential relationship is expressed as follows:

$$M_{xy}(t) = M_0 e^{-t/T2} \tag{2.1}$$

Where $M_{xy}(t)$ is the transverse magnetic moment at time t for a sample that has M_0 transverse magnetization at t=0. Since e^{-1}=0.37 when t=T2, then M_{xy}=0.37M_0.

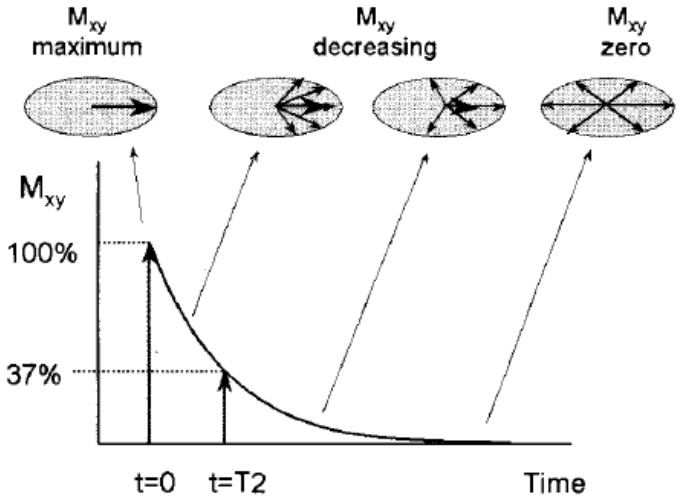

Figure 2.2: The loss of Mxy phase coherence occurs exponentially and it is caused by intrinsic spin-spin interactions in the tissues, as well as extrinsic magnetic field inhomogeneities. The exponential decay constant, T2, is the time over which the signal decays to 37% of the maximal transverse magnetization (e.g., after a 90°pulse). Adapted from [10].

T2 decay mechanisms are determined by the molecular structure of the sample. Mobile molecules in amorphous liquids exhibit a long T2, because fast and rapid molecular motion reduces or cancels intrinsic magnetic inhomogeneities. As the molecular size increases, constrained molecular motion causes the microscopic magnetic field variations to be more readily manifested and T2 decay to be more rapid. Thus large, nonmoving structures with stationary magnetic inhomogeneities have a very short T2 [10].

The loss of transverse magnetization (T2 decay) occurs relatively quickly, whereas the return of the excited magnetization to equilibrium (maximum longitudinal magnetization) takes a longer time. Individual excited spins must release their energy to the local tissue (the lattice). Spin-lattice relaxation is a term given to the exponential regrowth of M_z, and it depends on the characteristics of the spin interaction with the lattice (the molecular arrangement and structure). The T1 relaxation constant is the time needed to recover 63% of the longitudinal magnetization, M_z, after

a 90°pulse (when $M_z = 0$). The recovery of M_z versus time after the 90°RF pulse is expressed mathematically as follows:

$$M_z(t) = M_0(1 - e^{-t/T1}) \tag{2.2}$$

Where M_z is the longitudinal magnetization that recovers after a time t in a material with a relaxation constant T1. Figure 2.3 illustrates the recovery of M_z. Full longitudinal recovery depends on the T1 time constant.

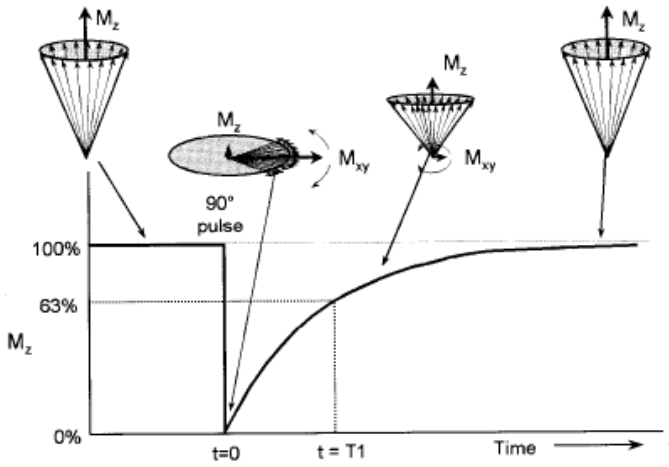

Figure 2.3: After a 90°pulse, longitudinal magnetization (M_z) is converted from a maximum value at equilibrium to zero. Return of M_z to equilibrium occurs exponentially and is characterized by the spin-lattice T1 relaxation constant. After an elapsed time equal to T1, 63% of the longitudinal magnetization is recovered. Spin-lattice recovery takes longer than spin-spin decay (T2). Adapted from [10].

T1 relaxation depends on the dissipation of absorbed energy into the surrounding molecular lattice. T1 relaxation is strongly dependent on the physical characteristics of the tissues - T1 ranges from 0.1 to 1 second in soft tissues, and from 1 to 4 seconds in aqueous tissues and water. Consequently, for solid and slowly moving structures, low-frequency variations exist and there is little spectral overlap with the Larmor frequency [10].

2.3 Spin Echo

Spin echo describes the excitation of the magnetized protons in a sample with an RF pulse and production of the FID, followed by a second RF pulse to produce an echo. The timing between the RF pulses allows separation of the initial FID and the echo and the ability to adjust tissue contrast.

An initial 90°pulse produces the maximal transverse magnetization, M_{xy}, and places the spins in phase coherence. The signal exponentially decays due to intrinsic and extrinsic magnetic field variations. After a time delay of $TE/2$, where

TE is the time of echo, a 180°RF pulse is applied, which inverts the phase of the spin system and induces a rephasing of the transverse magnetization. The spins are rephased and produce a measurable signal at a time equal to the TE. This sequence is depicted in the rotating frame in Figure 2.4.

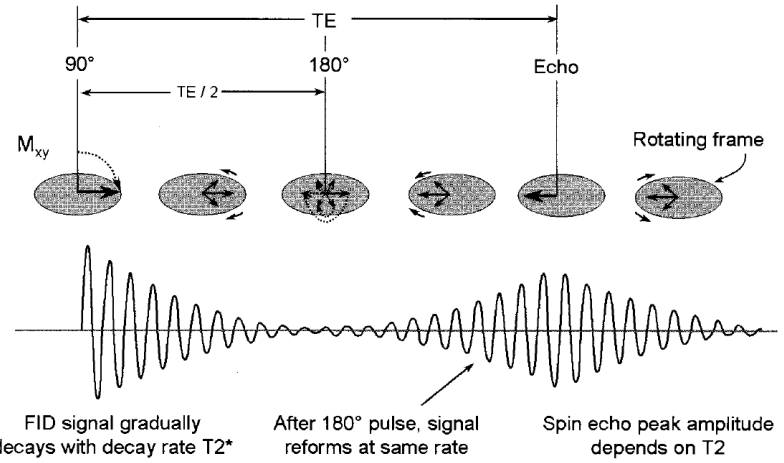

Figure 2.4: The spin echo pulse sequence starts with a 90°pulse and produces an FID signal that decays according to $T2^*$. After a delay time equal to $TE/2$, a 180°RF pulse inverts the spins and reestablishes phase coherence, producing an echo at a time TE. Effects of inhomogeneities of external magnetic fields are canceled, and the peak amplitude of the echo is determined by T2 decay. The rotating frame shows the evolution of the vector in the opposite direction of the FID. Adapted from [10].

Just before and after the peak amplitude of the echo (centered at time TE), digital sampling and acquisition of the signal occurs. Spin echo formation separates the RF excitation and signal acquisition events by finite periods of time, which emphasizes the fact that relaxation phenomena are being observed and encoded into the images. Contrast in the image is produced because different tissue types relax differently (based on their T1 and T2 characteristics).

Multiple echoes generated by 180°pulses after the initial excitation allow the determination of the "true" T2 of the sample. Signal amplitude is measured at several points in time, and an exponential curve is fit to this measured data (Figure 2.5). The T2 value is one of the curve-fitting coefficients.

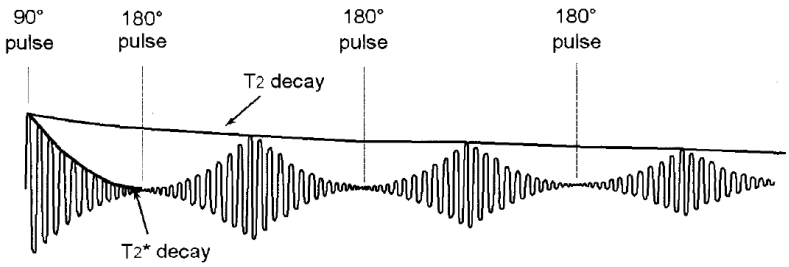

Figure 2.5: "True" T2 decay is determined from multiple 180°refocusing pulses. While the FID envelope decays with the $T2^*$ - decay time resulting from both intrinsic and extrinsic magnetic field variations, i.e. MR contrast materials, paramagnetic or ferromagnetic objects – decay constant, the peak echo amplitudes of subsequent echoes decay exponentially with time, according to the T2 decay constant. T2 is always longer than $T2^*$. Adapted from [10].

Contrast in an image is proportional to the difference in signal intensity between adjacent pixels in the image, corresponding to two different voxels in the subject.

2.4 T2-weighted image

A "T2-weighted" (T2W) spin echo sequence is designed to produce contrast chiefly based on the T2 characteristics of tissues by de-emphasizing T1 contributions. This is achieved with the use of a long Repetition Time (TR) to minimize the differences in longitudinal magnetization during the return to equilibrium, and a long TE to accentuate T2 differences during signal acquisition. Compared with a T1-weighted image, inversion of tissue contrast occurs, because short-T1 tissues usually have a short T2, and long-T1 tissues have a long T2. Tissues with a long T2 maintain transverse magnetization longer than short-T2 tissues, and thus present higher signal intensity. As TE is increased, more T2 contrast is achieved, at the expense of a reduced transverse magnetization signal.

2.5 Steady-State Precession

Steady-state precession refers to equilibration of the longitudinal and transverse magnetization from pulse to pulse in an image acquisition sequence. In all standard image techniques (e.g., spin echo), the repetition period TR of RF pulses is too short to allow recovery of longitudinal magnetization equilibrium, and thus partial saturation occurs. When steady-state partial saturation occurs, the same longitudinal magnetization is present for each subsequent pulse. For very short TR, less than the $T2^*$ decay constant, persistent transverse magnetization also occurs. During each pulse sequence repetition, a portion of the transverse magnetization is converted to longitudinal magnetization and a portion of the longitudinal magnetization is converted to transverse magnetization. Under these conditions, steady-state longitudinal and transverse magnetization components coexist at all times in a dynamic equilibrium. Steady-state imaging is practical only with short and very short TR. In these two regimes, flip angle has the major impact on the contrast "weighting" of the resultant images [10].

2.6 Cardiac Magnetic Resonance

MRI is used to make images of various organs of the human body, and specifically Cardiac Magnetic Resonance (CMR) imaging has emerged as a robust medical imaging technique for the non-invasive investigation of cardiovascular system function, structure and disorders. This MRI branch uses the same basic principles as MRI with the combination of rapid imaging techniques or sequences. CMR allows for the possibility of electrocardiography (ECG) gating and synchronization that enhances the quality of the images of the cardiovascular system by minimizing cardiac motion artifacts. With these optimizations, morphological structures and key functions of the cardiovascular system can be visualized and measured. The possibilities that the new applications allow, have created great enthusiasm in the CMR community. However due to the low number of studies yet performed, there is some uncertainty regarding its possible clinical applications. One of the possibilities that CMR opens

up is to provide a comprehensive assessment of cardiovascular disorders in a single session. Due to this, CMR represents a very important method of evaluation for the cardiac function and perfusion and can be used for many purposes in cardiology. Apart from these applications, an exceptional advantage of CMR is the capacity to do an exhaustive myocardial tissue characterization [11].

CMR is the only non-invasive imaging technique that can detect myocardial edema, which is believed to be a fundamental response to ischemia reperfusion injury. This has traditionally been performed with water-sensitive T2-Weighted (T2W) imaging, under the principle that prolonged T2-relaxation time due to increased mobility of water protons in edematous myocardium results in increased T2 signal intensity.

Studies in animals and patients have demonstrated that increased myocardial T2 may be associated not only with acute myocardial infarction (MI), but also with severe transient myocardial ischemia [12]. Elevated myocardial T2 is also known to accompany myocarditis, cardiac allograft rejection and sarcoidosis, among other conditions [2]. This relationship makes T2 and T2W imaging very useful in CMR and can be clinically helpful to differentiate acute from chronic myocardial lesions and to detect even small acute myocardial damage very early [13]. Differences in myocardial T2 relaxation should reflect differences in the underlying tissue characteristics.

These and other studies using T2 to characterize pathological changes in myocardium have relied on T2W imaging with a black-blood (BB) turbo spin echo technique [14]. Traditional BB turbo spin echo-based T2W imaging is limited by a set of challenges which continue to affect its diagnostic utility (Figure 2.6) and impede its widespread clinical acceptance: i) phased-array coils cause regional myocardial signal variation that can lead to inaccurate interpretation and diagnosis – thus specialized normalization methods are required; ii) high/bright signal from stagnant blood makes it difficult to differentiate edema from sub-endocardial blood; iii) myocardial signal loss caused by through-plane motion; and iv) the qualitative nature of T2W imaging where interpretation depends on regional differences in myocardial signal intensity, which may vary depending on sequence parameters (e. g. TE, slice thickness). In patients with irregularities in cardiac rhythm or difficulties with breath holding, artifacts can increase.

In order to solve these problems, semi-quantitative approaches have been developed for T2W-CMR that, for instance, compute signal intensity relative to unaffected remote myocardium or adjacent skeletal muscle. However, these approaches perform poorly when there is diffuse myocardial involvement. Furthermore, these may be insensitive when there is concomitant skeletal muscle involvement, which has been reported in myocarditis [15].

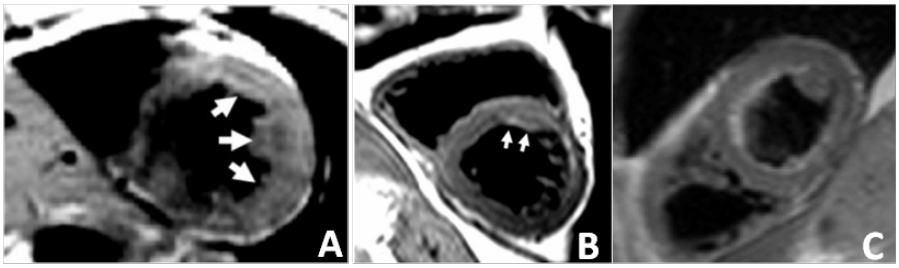

Figure 2.6: A: Acute myocardial infarction (MI) patient, with significant RR variability, exhibiting edema with false-positive black-blood (BB) turbo spin-echo showing apparently elevated T2 in the left anterior descending (incorrect) coronary territory. B: Patient with chronic MI in the left anterior descending territory showing a false-positive BB turbo spin-echo suggesting edema. C: Example illustrating bright-blood artifact for BB turbo spin-echo image resulting from stagnant blood within trabeculae along the endocardial wall. Adapted from [16].

Therefore alternatives for more stable detection and easier quantification of edema are clinically warranted. An alternative approach to T2W imaging, which overcomes many of these limitations, is to directly quantify the T2 of the myocardium – quantitative T2 mapping.

2.7 T2 MAPPING

In recent years, new 'mapping' techniques have been proposed to allow for quantitative CMR. The majority of these sequences are normally single-slice breath-hold (BH) acquisitions. Using such mapping techniques, instead of generating 'weighted' images, a colored pixel map is produced where each pixel corresponds to the T1, T2 or $T2^*$ value (Figure 2.7). With the right contrast agent, it is also possible to use these maps to analyze the interstitium (e.g. amyloid, edema or fibrosis) and evaluate the extracellular volume (ECV) [17].

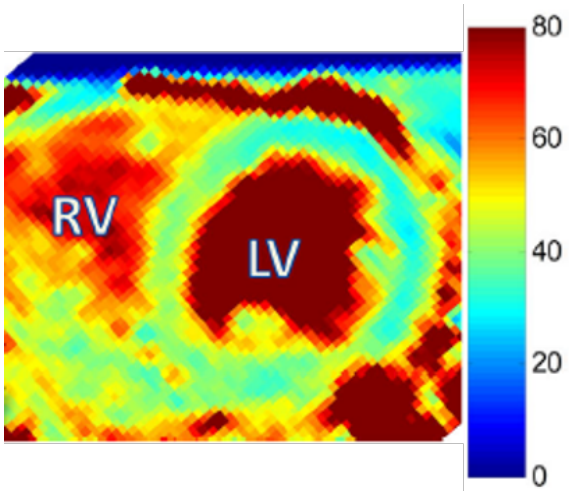

Figure 2.7: T2 mapping in healthy volunteer demonstrates a homogeneous T2 distribution. Mid-ventricular short-axis (SAX) slice through the left ventricle (LV) shows homogenous T2 values throughout the myocardium. It is also possible to see the right ventricle (RV). In this study the average myocardial T2 value was 40.5 ± 3.3 ms. Adapted from [18].

T2 mapping is based on several snapshot images with different TEs (T2 weighting) and a map is generated that gives T2 time in absolute value for every single pixel. In a colour-coded scale, the map directly displays absolute T2 values for any single pixel that can be assessed globally or for any segment or region of interest (ROI). The map can be acquired in any orientation and is independent from coil proximity.

There are 2 main types of T2 mapping techniques: spin-echo-based and T2-preparation (T2prep) steady-state free-precession (SSFP)-based techniques. However, since the T2 mapping techniques based on spin-echo sequences are sensitive to ghosting and motion artifacts (induced by cardiac arrhythmias or imperfect BH), the latter are generally preferred in CMR [3].

Normally, a T2prep SSFP sequence [16] is used to generate three T2W images – the minimum required for an exponential fit and to minimize BH duration and patient discomfort – each one with a different T2prep time. Because these images are acquired in the transient state of single-shot SSFP immediately after the T2prep pulse, the primary source of contrast is the T2 relaxation time. Thus, the signal in each image represents a different TE along the T2 decay curve.

The design of this sequence incorporates non-selective composite pulses for insensitivity to motion and B_0 and B_1 inhomogeneities and the SSFP readout module is usually applied immediately after the T2prep module to sample the magnetization prior to it reaching the steady state.

Parametric maps are generated by fitting the measured signal in each pixel to the following two-parameter (M_0 and T2) exponential equation:

$$S(x,y) = M_0(x,y)e^{-TE_{T2prep}/T2(x,y)} \tag{2.3}$$

where S(x,y) is the measured signal intensity, M_0(x,y) is a lumped parameter that includes the equilibrium magnetization and local receiver coil sensitivity, and TE_{T2prep} is the T2prep echo time (Figure 2.8). Those TE_{T2prep} times are chosen based on the expected range of T2 values in the myocardium – recent work has shown that the T2 for normal myocardium is approximately 55 ms [4]. Longer TE_{T2prep} than the T2 for normal myocardium can cause significant signal loss.

Using quantitative T2 mapping, the artifacts associated with T2W imaging may be minimized, image contrast dependency on user-defined parameters and subjective interpretation can be reduced, and subtle T2 differences between tissues may be more easily detected. Also the quantitative approach is independent of the heart rate, and has low interscan variability rates [19]. The quantification of T2 offers a distinct advantage in the detection of global changes, in comparison with T2W imaging, which relies on regional differences in myocardial signal.

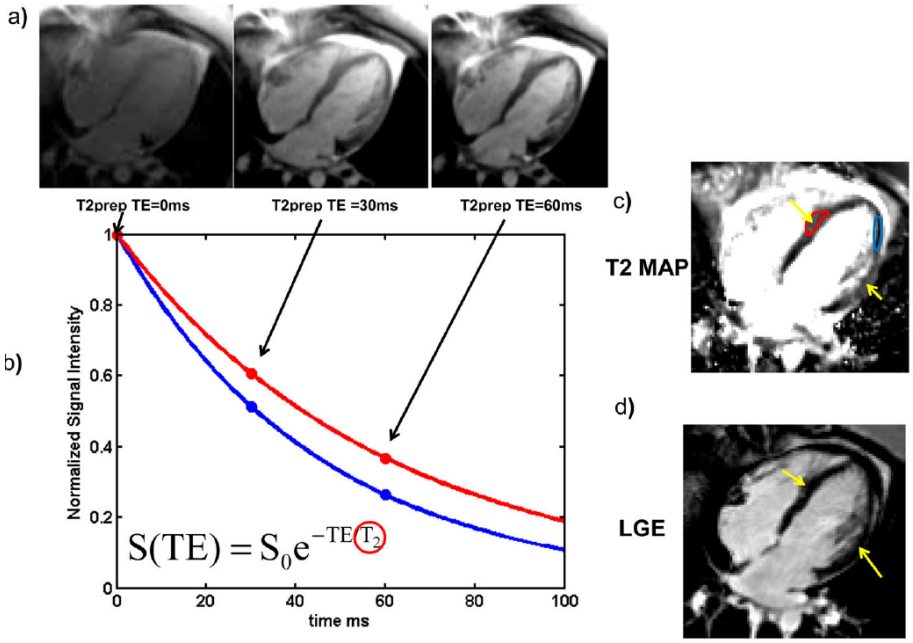

Figure 2.8: Calculation of T2 maps using a T2prep pulse sequence in a patient with atypical Takusubo cardiomyopathy. (a) Multiple images with T2 preparations with different TE are acquired. As the TE is increased for this spin-echo-based preparation, the myocardial signal intensity decreases due to T2 decay. (b) A T2 decay curve is fit to the data of each pixel, with pixels with longer T2 (red curve) decaying more slowly than regions with shorter T2 (blue curve). (c) The T2 map shows a region of edema (yellow arrows and red region of interest (ROI)) in this patient. (d) The absence of late gadolinium enhancement (LGE) confirms the diagnosis of atypical Takusubo cardiomyopathy. Adapted from [3].

Quantitative T2 mapping addresses the limitations of qualitative T2W imaging and provides a practical, promising and accurate method of assessing myocardial edema associated with acute ischemia, infarction, and other pathological conditions affecting myocardial water content and showing promise for application in clinical practice. The lack of sensitivity to field inhomogeneities makes T2 mapping a good strategy for the detection of regional hemodynamic differences in the heart. To perform T2 mapping, a cardiac imaging method that would provide high T2 contrast, high signal-to-noise ratio (SNR), and low motion sensitivity is thus highly desirable.

As with T1 mapping, global diseases such as pan-myocarditis may be identified by T2 mapping, and preliminary results showing this in several rheumatologic diseases (lupus, systemic capillary leak syndrome) and transplant rejection, detecting early rejection missed by other modalities [5].

2.8 T2 PREPARATION MODULE

The most common approach for achieving T2 weighting for T2 mapping in CMR uses the T2prep module. A magnetization-prepared, T2W sequence is used to suppress muscle and venous structures. When combined with lipid suppression, this technique improves the visualization of the coronary arteries. The T2prep module is shown in Figure 2.9 and was designed to store T2W magnetization along M_z in a manner that is robust in the presence of flow as well as B_0 and B_1 inhomogeneities and may be combined with virtually any imaging technique. A 90_x°excitation is

followed by a train of 180_y°pulses, which are equally separated. After the refocusing pulses a 90_x°tip-up pulse is performed to return the transverse magnetization to the longitudinal axis, followed by a spoiler gradient (SPGR) to destroy any residual transverse magnetization.

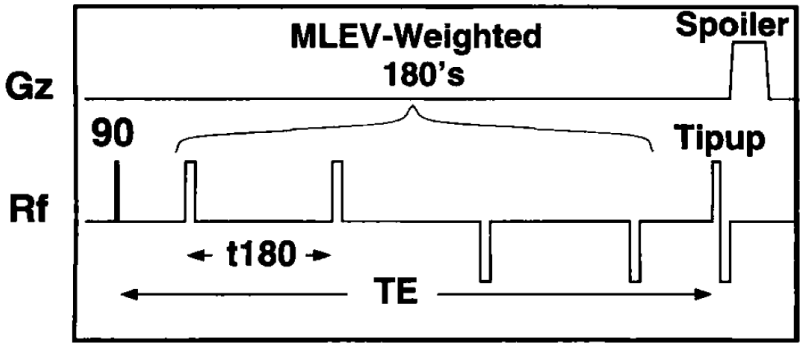

Figure 2.9: T2prep sequence illustrated with four refocusing pulses.

The T2 weighting generated by this module suppresses muscle because the T2 of muscle is much shorter than that of oxygenated blood (e. g. $T2_{\text{oxygenated blood}} = 290$ ms, $T2_{\text{myocardium}} = 40$ ms) [20]. After the application of the first 90°RF pulse of the T2prep module, the M_{xy}°magnetizations of the vessel wall and fat decay faster than that of blood because of their shorter T2 relaxation time, thereby increasing the contrast between them. Conveniently, the T2 of oxygenated blood is also greater than that of venous blood which improves contrast between oxygenated and de-oxygenated blood.

2.9 Respiratory Navigators and Motion Correction

Respiratory navigators are incorporated into the MRI pulse sequence and can be used to monitor the respiratory movement and deformation of the heart and surrounding tissues and organs (Figure 2.10).

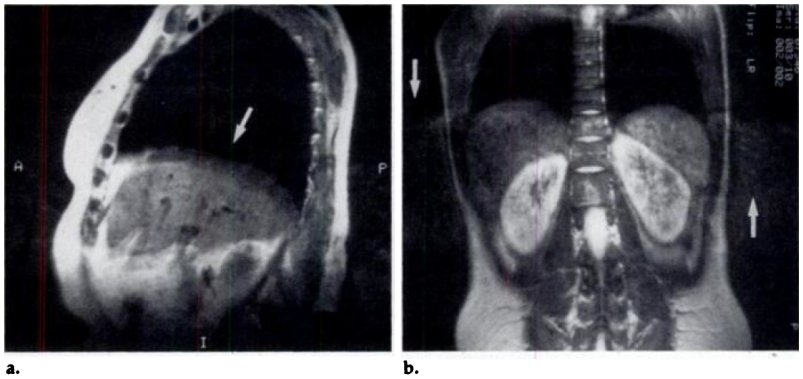

Figure 2.10: Respiratory motion can cause different effects. Craniocaudal respiratory motion of the diaphragm and abdominal organs (e.g. liver and spleen) can produce blurring in the top of the abdomen and in the liver (see arrow in image (a)) and ghost images of these organs (see arrow in image (b)). Temporal modulation of the magnitude and phase of the transverse magnetization, as tissues move from voxel to voxel, are the responsible for these effects. Adapted from [21].

Respiratory navigators are normally real-time image acquisitions, which are interleaved with the high resolution MR sequence, allowing snap-shots of one or more motion dimensions of the respiratory state before or after each segmented k-space acquisition.

Ehman et al. [21] in the end of the 1980's proposed the first respiratory diaphragmatic one-dimension navigator (d1D NAV) which was obtained on the top of the right hemi-diaphragm, determining the foot-head (FH) motion of the lung-liver interface to correct for the respiratory motion of the liver. Due to its characteristics – it can be used with a large amount of cardiovascular imaging sequences, it is easy to use and allows a very accurate tracking of the lung-liver interface – this became a very popular way to assess the respiratory motion for CMR [6]. Also the possibility of prospective real-time motion compensation, because of the time of acquisition and processing being relatively short (around 10-30 ms), is a major advantage of the d1D NAV. In addition to this, as the respiratory motion is mainly perpendicular to the lung-liver interface (i.e. in the FH direction) with the d1D NAV approach the motion can be followed with very good precision.

The d1D NAV can be implemented using two alternative approaches: a spin-echo implementation where the 90°RF excitation and 180°RF refocusing pulses are obliquely aligned (the overlapping zone is the d1D NAV volume) or a pencil beam navigator – 2D RF excitation pulse with a SPGR echo read-out in the orthogonal direction. Figure 2.11 shows scan planning for the two approaches, as well as the resulting d1D NAV signal also represented over time, where it is possible to see the respiratory motion between the lung and the liver. However, hysteresis between the diaphragm and the heart respiratory motions between inspiration and expiration, and the necessity of a motion model to estimate the respiratory motion of the heart (indirectly measured using the diaphragm movement information), are the main limitations of the d1D NAV.

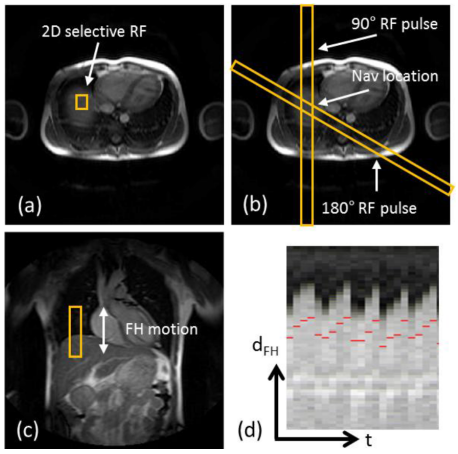

Figure 2.11: Scan planning of d1D NAV in axial plane using either a 2D selective RF "pencil beam" excitation (a) or a spin-echo approach with obliquely aligned 90°excitation and 180°refocusing pulses (b). The d1D NAV is located on the dome of the right hemi-diaphragm with the read out in the foot-head (FH) direction (c). The d1D NAV signal (d) clearly shows the displacement of the lung-liver interface along the FH direction (dFH) over time (t). Adapted from [6].

Additionally, for using the d1D NAV it is necessary to do scan planning and also define separate imaging parameters for the navigator acquisition, which increases the scan complexity making it an inherent limitation. In order to address these disadvantages, a new technique for respiratory motion compensation has been proposed: so called self-navigation (Figure 2.12) [7]. It consists of an estimation of the respiratory motion directly from the MR data, respecting certain conditions: the central line of k-space is measured at least once per k-space segment and in order to maximize the accuracy of the respiratory motion, the readout must be in line with the FH direction. With this technique, the problems associated with hysteresis among diaphragmatic and heart motion do not exist because the respiratory motion is directly measured instead of resorting to a motion model [8].

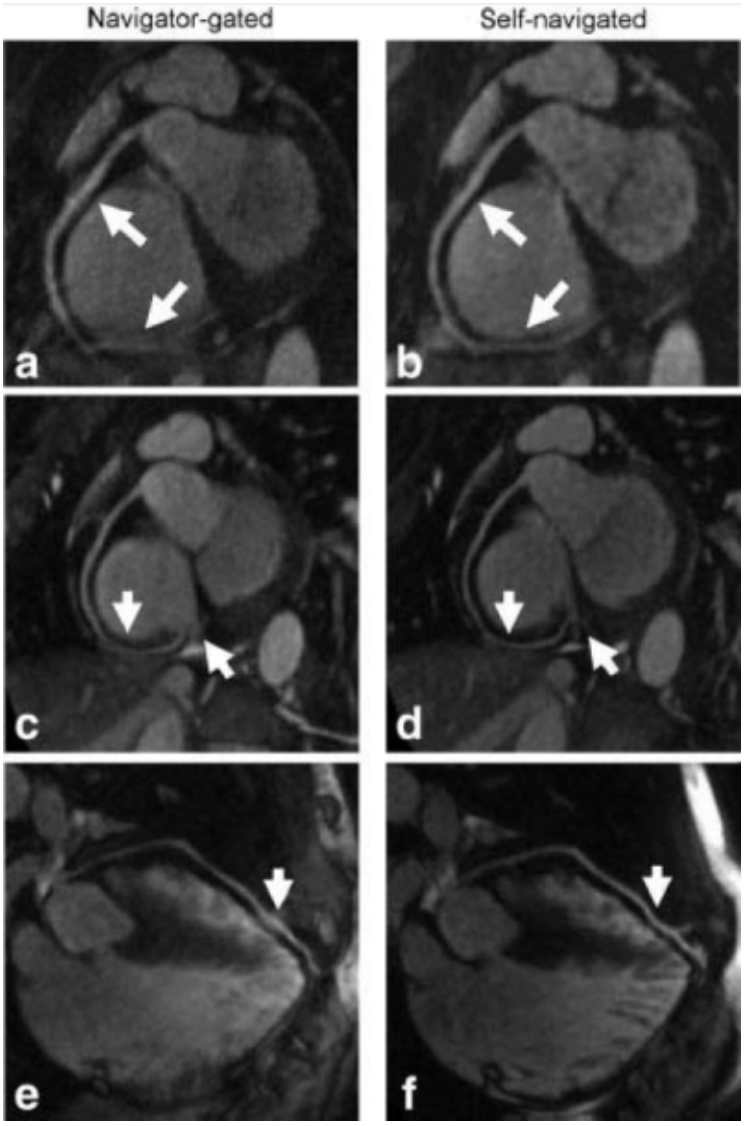

Figure 2.12: Reformatted images of the right coronary acquired with the d1D NAV technique (a, c) and with the self-navigation (b, d). In (a) and (b) the proximal and the distal part of the right coronary artery are highlight with the white arrows. It can be observed that with self-navigation the vessel sharpness and length are increased. The white arrows in (c) and (d) highlight regions where the self-navigation showed an improved delineation of the coronary vessels where similar image quality was obtained with both approaches. Adapted from [7].

Normally, static tissue (e.g. chest wall) is present in the navigator image because self-navigation images are acquired as 1D projections of the FOV, so the motion estimation performance of the navigator can become compromised. To overcome this limitation, a combination of this method with spatial encoding has been proposed which separates moving from static tissue, which is called image-based navigation (iNAV).

In iNAV single two-dimensional (2D), orthogonal 2D, or three-dimensional (3D) [9] real-time images are acquired in every heart-beat preceding the main MR acquisition (Figure 2.13). With this technique it is possible to improve the quality of the respiratory motion estimation because the moving heart can be spatially isolated from surrounding static tissues. Beside this advantage, image-based motion compensation has extra degrees of freedom for motion correction, and so rotation and non-rigid motion correction are also possible – not limited to only translational motion in numerous directions. However, the navigator acquisition can saturate the magnetization or artifacts may be present in the subsequent and spatially overlapping MR acquisition, when the iNAV is used. A solution may be placing the MR acquisition before the navigator image, so called trailing navigator, but this cannot be combined with prospective respiratory gating and correction. When iNAV is compared with 1D navigators (e.g. d1D NAV or self-navigation), it is easy to imagine that those real-time implementations are much more challenging, due to the augmented computational complexity of multi-dimensional image reconstruction, registration and correction. The downside of iNAV compared to self-navigation, is that extra scan planning is required to define the navigator image location, because the navigator is not easily extracted from image acquisition.

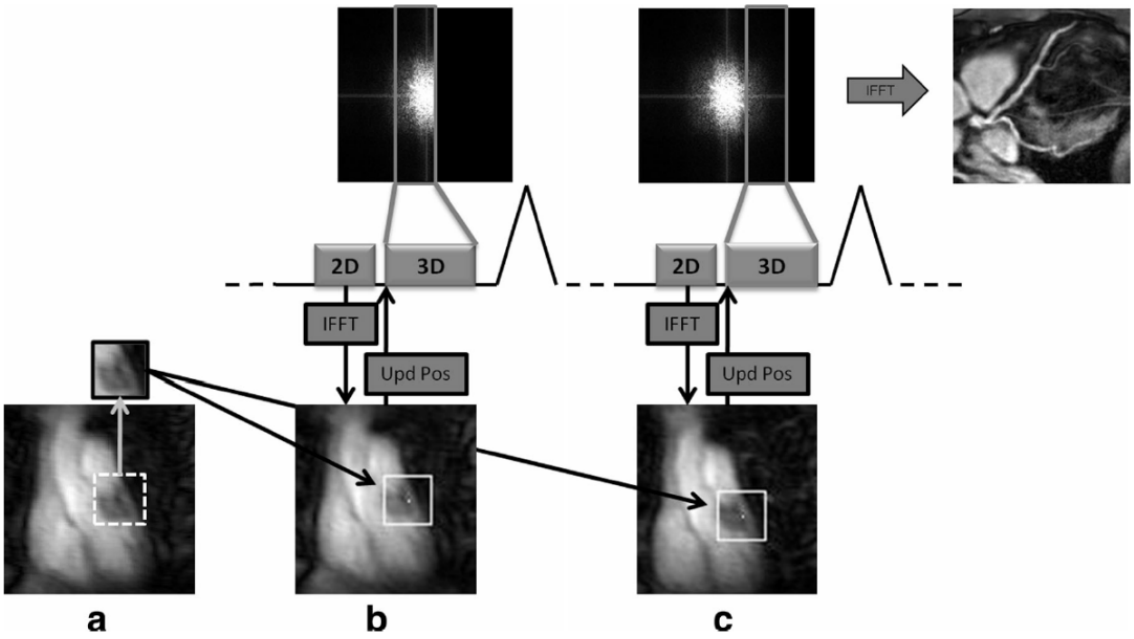

Figure 2.13: 3D segmented k-space CMR angiography sequence using iNAV for prospective motion correction. Image (a) is the reference and the template is extracted from it. After that it is utilized to estimate 2D motion in the shots (b) and (c). Prior to each acquisition, the position of the 3D image is updated using this information. Adapted from [9].

As previously stated, image-based approaches have been suggested to improve motion estimation, by spatially encoding in 2D or 3D [22], which enables the possibility to separate the static chest from the moving heart. However, Henningsson et al. [23] created a 2D self-navigator (2DSN) which acquires images by encoding the startup profiles of a balanced SSFP sequence, which are principally used to catalyze the magnetization towards the steady-state. This makes possible the translational correction in the frequency and phase encoding directions and makes possible the separation of static and moving structures. In this approach a template matching algorithm was used to estimate the respiratory motion from the 2DSN and during the image reconstruction the data is retrospectively corrected. With this approach the FH and left-right (LR) motion are calculated and retrospective translational motion correction performed.

In this approach, the 2DSN image resolution in the phase encoding direction is a function of the number of startup profiles. All 2DSN are reconstructed to the same matrix size irrespective of the phase encoding resolution. The 3D imaging volume is oriented in the coronal plane with frequency encoding in the FH direction and phase encoding in the LR direction. In order to increase the 2DSN resolution and at the same time diminish the duration of the 2DSN, a half Fourier acquisition with a factor of 0.6 in the phase encoding direction can be used [24]. As the acquisition of iNAV center of k-space should be as close to the 3D image acquisition as possible, the 2DSN sequence is implemented with a high-low profile order. Also, along the slice selection direction no phase encoding is needed and so 2DSN images are projections of the field-of-view (FOV) in the anterior-posterior direction.

In the CMR sequence, it is possible to create image contrast by using prepulses such as fat saturation or T2prep (used for T2 mapping). The number of startup profiles determines the time between prepulses and imaging and so it is desirable to minimize this time. Also k-space data is modulated with a linear phase – in the image domain it represents a translational shift – so the motion correction can be applied to the CMR retrospectively. The phase shift φ_{A} introduced by the motion along encoding direction A can be calculated for the shot s, as:

$$\varphi_A(s) = (2\pi \cdot \Delta A)/FOV_A \tag{2.4}$$

where ΔA is the displacement estimation as measured by the navigator, and $\mathrm{FOV_A}$ is the field of view. The phase modulation is applied to each complex k-space data point $\mathrm{k_j}$, where j is the index in k-space along encoding direction A, acquired in shot s as described by

$$k_j = k_j \cdot e^{(i \cdot \varphi_A(s) \cdot j)} \tag{2.5}$$

For the above mentioned correction techniques the phase shift is calculated for every shot in the frequency encoding direction.

Henningsson et al. [23] concluded that with their 2DSN the image quality of CMR was improved compared to a d1D NAV with a FH tracking factor of 0.6. Ten

startup profiles were shown to be sufficient for 2DSN motion correction and to generate CMR with excellent image quality.

2.10 T2 mapping – State of the art

Over the past 25 years a number of in vivo studies have measured the T2 of healthy human myocardium, primarily using techniques based on spin echo acquisitions. These methods are time-consuming and prone to the same motion sensitivity that has plagued T2W imaging of the heart. Also, T2 mapping techniques based on BB turbo spin echo sequences are sensitive to ghosting and motion artifacts [3].

Myocardial T2 mapping techniques using T2prep SSFP have been described by Huang et al. [25] for blood oxygenation level-dependent (BOLD) imaging – which is the detection of local T2 or $T2^*$ changes in the myocardium in response to a vasodilatory challenge. A combined T1 and T2 mapping method by Blume et al. [26] for differentiation of acute from chronic MI was proposed. Blume et al. [26] showed that myocardial T2 estimation is improved by including an image without T2prep (TE = 0 ms). While these were promising initial studies, neither investigated the potential for T2 mapping to address the known limitations of T2W imaging caused by residual blood signal, surface coil intensity variation, and myocardial motion artifact.

In 2009, Giri et al. [4] introduced a direct T2 mapping for quantitative measurement of T2 relaxation time, using T2prep SSFP and showed improved results compared with the conventional T2W (Figure 2.14). Giri et al. have demonstrated an accurate, fast, quantitative approach to detect the elevated T2 associated with myocardial edema that successfully addresses the limitations of T2W imaging.

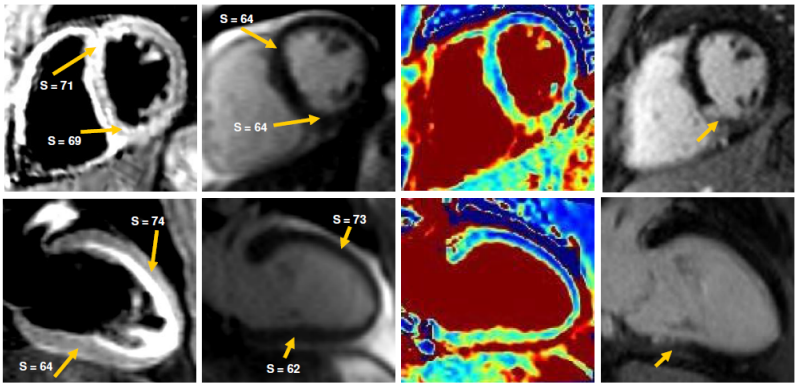

Figure 2.14: Mid-ventricular short-axis and vertical long axis images from a patient. Coronary angiography confirmed >90% occlusion of right coronary. The infracted region could not be detected in T2prep SSFP image with T2prep = 55 ms (column 1). T2 maps (column 2) demonstrate increased T2 in the inferior regions and the endocardial borders are clearly demarcated. Late Gadolinium Enhancement (LGE) images (column 3) show the location and extent of the infarct. S = Signal Intensity. Adapted from [4].

In this approach, a T2-prepared SSFP sequence was used to produce three T2W images, one each with different T2prep times (TE_{T2prep} = 0, 24 and 55 ms). The

principal source of contrast is the T2 relaxation time because these images are obtained in the transient state of single-shot SSFP immediately after the T2prep pulse. The SSFP readout module was applied immediately after the T2prep to sample the magnetization prior to reaching the steady state. A wait time of 2 RR intervals was introduced between the images to allow for relaxation of longitudinal magnetization. Therefore, a total of 7 RR intervals were necessary to get the three T2prep images. The sequence timing was adjusted for each T2prep time to guarantee that the SSFP readout was always timed to the same phase of the cardiac cycle.

Many studies were performed based on this sequence and they have shown that T2 mapping can detect edematous myocardial territories in a variety of cardiac pathologies, including acute MI [19] and it also has been used to identify iron overload [27]. Verhaert et al [28] assessed T2 mapping in patients with acute MI and found that myocardial segments characterized by recent ischemic injury can be quantitatively differentiated from remote myocardium by their higher T2 value. Another study from the same group [5] showed the usefulness of T2 mapping in suspected myocarditis or tako-tsubo cardiomyopathy, demonstrating that T2 mapping can identify myocardial involvement beyond conventional CMR techniques such as T2W and Late gadolinium enhancement (LGE) imaging. T2 mapping has also been used as a non-invasive tool for cardiac transplant monitoring with promising preliminary findings in small cohorts and also shown to be a potential non-invasive tool for characterizing rejection in cardiac allografts [29]. Finally, T2 mapping might help to improve tissue characterization in the case of intracardiac tumour but more experience across various tumour entities is needed to assess the clinical utility of T2 mapping for tumour differentiation [30].

Unfortunately, these T2 mapping techniques exhibit heart-rate dependency, sensitivity to the order of acquisition and flip angle, incomplete T1 recovery resulting in T1 weighting and errors in the T2 relaxation time measurements [31]. Also, with this technique, T2 maps are typically acquired as one or several 2D slices, while the underlying pathologies often have a complex 3D structure. In addition, a 3D approach should sample considerably more myocardial tissue per unit time than a 2D approach, and might thus increase the precision of T2 determination – the 2D approaches have limited in-plane resolution [4], [28].

The value of higher field strength for clinical imaging has previously been demonstrated for selected CMR applications and is mostly due to the higher SNR and thus higher spatial and temporal resolution, which allow for improved sensitivity and specificity [32]. For the first time, van Heeswijk et al. [33] validated a free-breathing radial gradient echo T2 mapping technique at 3T, demonstrating its accuracy and reproducibility in comparison to a BH BB T2W fast spin echo technique. van Heeswijk et al. [18] also achieved 3D T2 maps at 3T using a 3D radial acquisition in combination with golden step-based self-navigation. Using a bSSFP sequence with 20% undersampling resulted in isotropic images (1.7 mm^3). Imaging every other heartbeat recovered SNR, and the residual influence of T1 was corrected by an empirical factor applied during fitting. All data acquired were used, and 3D affine warping of volumes at different respiratory positions was used in final image reconstruction.

van Heeswijk et al. tested it in a small group of 11 patients where comparisons were made regarding the extent of edema assessed by conventional T2W images and T2 maps at 3T (Figure 2.15). This technique allows for the 3D characterization of edema in established cardiovascular disease in less than 20 minutes and the performance of this 3D T2 mapping approach appears to be a robust tool for myocardial edema at 3T as well as at 1.5T.

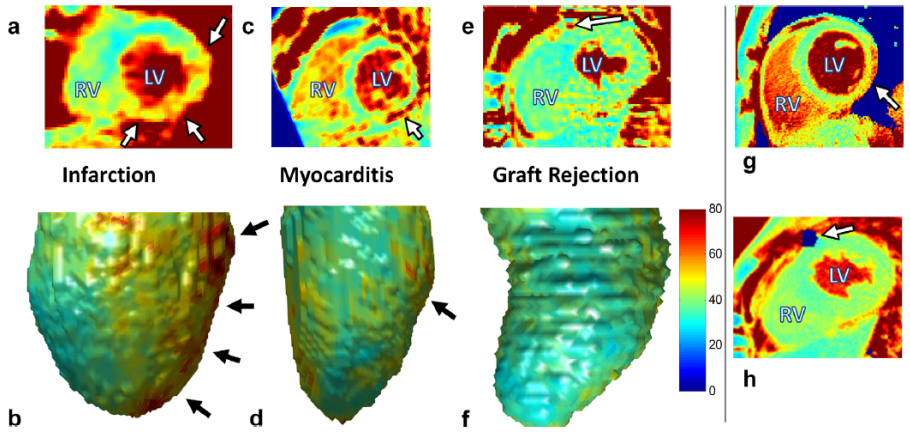

Figure 2.15: Short-axis (SAX) slices and 3D volume renderings of the 3D T2 maps in three patients with cardiovascular diseases. a, b: A patient with a subacute MI. A region with significantly elevated T2 can be identified (arrows). c, d: A patient with myocarditis. Several small regions of T2 elevation can be discerned (arrows). e, f: A patient with a cardiac graft and no rejection as seen in endomyocardial biopsy also demonstrates the absence of subendocardial elevated T2 values, although a small patch with elevated T2 can be observed at the anterior epicardium (arrow). g: A region of elevated T2 can be observed in a control 2D T2 map at the same level as (c). However, the region is mostly epicardial and not transmural, which causes it to appear smaller in the 3D subendocardial segmentation. h: A control 2D T2 map at the same level as (e). The blue patch is a nonmapped signal void. Adapted from [18].

van Heeswijk et al. work represents a significant contribution to the technical developments in parameter-mapping techniques. Specifically, their investigation provided further improvement to the assessment of myocardial edema beyond conventional T2W fast spin echo sequences or bright-blood T2prep module SSFP techniques. Techniques based on T2W SSFP are sensitive to susceptibility artifacts and large RF inhomogeneities affecting image quality. The need for longer BH times to enable T1 recovery between T2prep modules may also be a challenge for the clinical applicability of 3T CMR edema imaging. The introduction of free-breathing T2 mapping segmented k-space radial gradient echo may not only overcome some of the limitations described, but it may also provide a tool for accurate quantitative assessment of the change in tissue composition at 3T and to specifically assess myocardial edema. Mapping experiments in volunteers at 3T demonstrated that at higher field strengths myocardial T2 can be assessed with low intra- and inter-observer variability [34].

More recently, Ding et al. [17] developed a free-breathing 3D T2 mapping method based on the saturation-prepared, T2prep RF-SPGR echo sequence, which achieves high spatial resolution T2 maps with whole-heart coverage (Figure 2.16). Compared

with previous T2 mapping methods, this sequence is 1) less dependent on field homogeneity (obtained by using SPGR and partial echo readout), 2) highly efficient (by utilizing all heartbeats for imaging and requiring no T1 recovery time), 3) motion compensated (via respiratory navigators), 4) insensitive to heart rate variation (by using a "reset" nonselective saturation prepulse), and 5) intrinsically spatially registered by interleaving volumes with different T2prep. Also, the 3D acquisition improved both through-plane motion compensation and SNR compared with previous techniques.

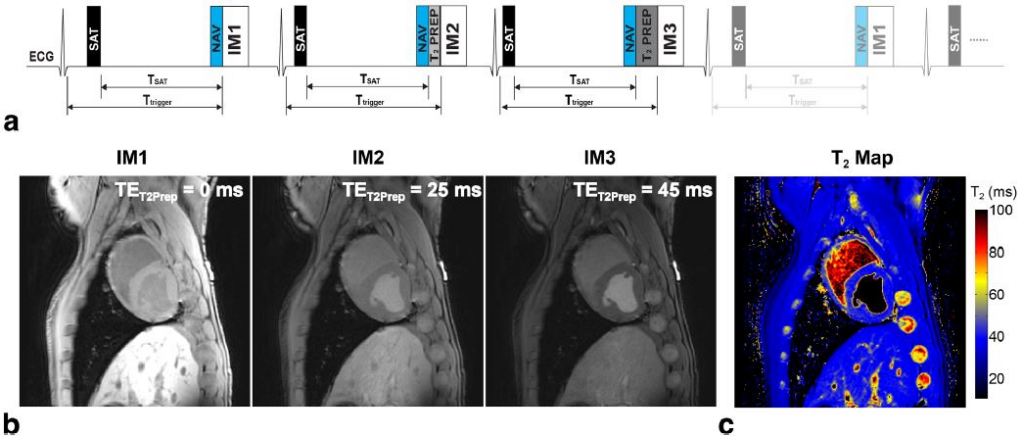

Figure 2.16: a: Pulse sequence diagram for the free breathing 3D T2 mapping sequence. Three or more differentially T2-weighted (T2W) volumes were acquired in an interleaved fashion. Each volume was respiratory navigator gated, ensuring coregistered images. A SAT pulse was applied at the start of every heartbeat to reduce variations in signal intensities. To prevent changing heart rates from affecting the degree of T1-weighting in the images, the T_{SAT} (SAT delay, duration between SAT and T2 Prep) was kept constant even when the $T_{trigger}$ (trigger delay, imaging delay after ECG R wave is detected) was allowed to change to maintain imaging during diastole in the presence of heart rate variability. The same navigator template was used for detection of motion across all volumes, ensuring coregistration. If a given heartbeat was rejected due to respiratory motion, data were reacquired immediately until an appropriate level of motion was achieved before proceeding to the next volume's data. b: Sample images from three acquired 3D volumes yielded voxel-by-voxel 3D T2 maps (c). Adapted from [17].

Finally Yang et al. [35] developed a time-efficient, free-breathing, whole heart T2 mapping technique at 3T with hybrid radial-cartesian trajectory. ECG-triggered 3D images were acquired with different T2 preparations at 3T during free breathing. Respiratory motion was corrected with a navigator-guided motion correction framework at near perfect efficiency and image intensities were used to fit a mono-exponential function to derive myocardial T2 maps. Yang et al. concluded that the proposed whole heart T2 mapping approach could be performed within 5 min with similar accuracy to that of the 2D BH T2 mapping approach.

Although, T2 maps can easily be acquired with higher hearts rates, in arrhythmias and also in other conditions when T2W imaging fails and allows for global and regional assessment of myocardial tissue properties, further technical improvements - e.g. the effects of scan time shortening techniques on the performance of T2 mapping - are expected to advance their clinical application in the detection of acute, subacute, and subclinical pathologies.

In so far T2 mapping represents a very promising tool for real world CMR in the acute clinical setting and has already demonstrated clinical usefulness as a quantitative tissue characterization MR technique in a variety of common cardiac conditions. T2 mapping appears to be a useful confirmatory test for conventional T2W imaging and is an emerging topic with the potential to become a powerful tool in the identification and quantification of diffuse myocardial processes without biopsy. Early evidences suggest that this technique detects initial stage disease missed by other imaging methods and has potential for prognosis, as a surrogate endpoint in clinical trials and also to monitor therapy.

Chapter 3

Material and Methods

This chapter contains a description of the pulse sequence details and data acquisition of the proposed imaging approach. It also contains an explanation regarding how motion estimation and correction are performed. The protocols for the phantoms and healthy subjects' studies are also described.

3.1 Pulse Sequence Details and Data Acquisition

The first phase of the pulse programming consisted of adapting an implementation for T1 mapping that already existed, adding adiabatic T2 preparation (T2prep) pulses with variable echo times (TE) to an image acquisition with multiple dynamics in order to implement a T2 mapping sequence. The T2prep sequence was setup for mid-diastolic acquisition, which is the most quiescent phase during the cardiac cycle, to minimize cardiac motion (Figure 3.1). The SSFP readout module was applied immediately after the T2prep to sample the magnetization prior to reaching the steady state.

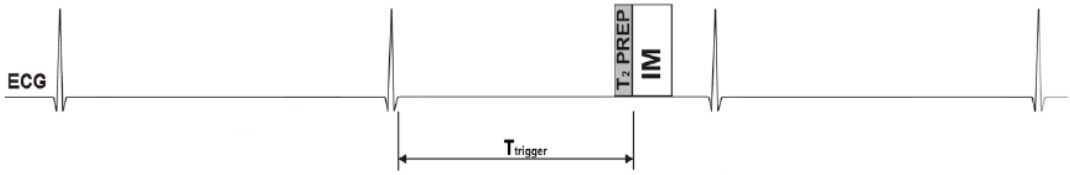

Figure 3.1: Representation of T2 preparation pulse (T2prep) position along the ECG. $T_{trigger}$ is the time from R-wave detection until the beginning of image acquisition (IM).

Sequence parameters (Figure 3.2) were added allowing the user to choose the number and duration (how many milliseconds the TE should increase along the different T2prep) of T2prep prepulses to be performed (Figure 3.3). In order to ensure a reasonable range of possible values, the user can only choose six different TE values, otherwise the scan time would be too long. To compensate for the change in duration of the T2prep, a condition was imposed that the ECG trigger delay – time from R-wave top until the beginning of image acquisition remained constant even when the duration of the T2 prep changed.

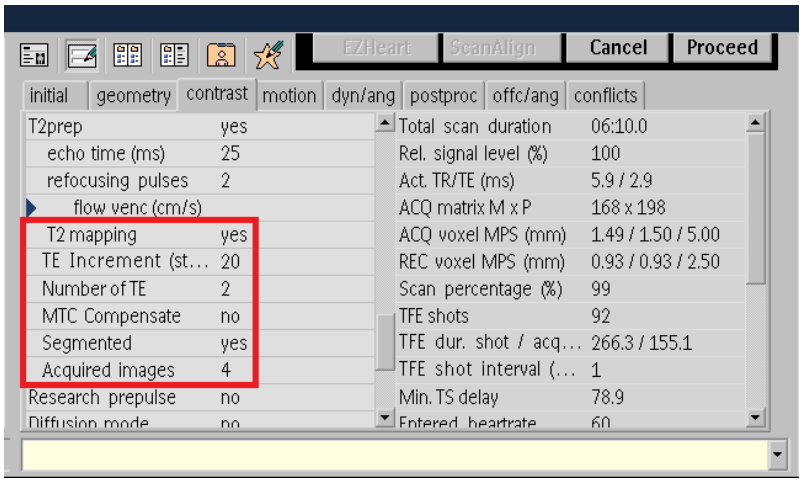

Figure 3.2: Display of the added parameters (red box). When the T2 mapping sequence is enabled, the user can choose parameters like the number of milliseconds for the increment in the echo time (TE) or the number of TEs to be performed.

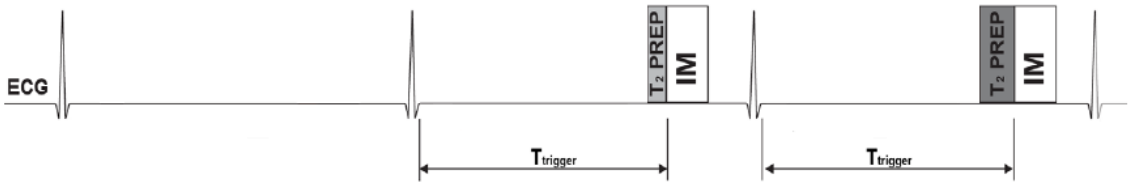

Figure 3.3: Pulse sequence diagram for the T2 mapping sequence. A maximum of six T2-weighted (T2W) volumes are acquired in an interleaved fashion with different TE values. The $T_{trigger}$ (trigger delay, imaging delay after ECG R wave is detected) was kept constant even when the TE_{T2prep} changed.

Once this was implemented, an extra acquisition was added at the beginning of the scan with a T2prep with zero TE (Figure 3.4). This non–T2-prepared volume (i.e. TE = 0 ms) has the highest SNR and it is used to increase image quality and allow better fitting of the data. In this particular dataset, more distal segments of the heart are not well depicted.

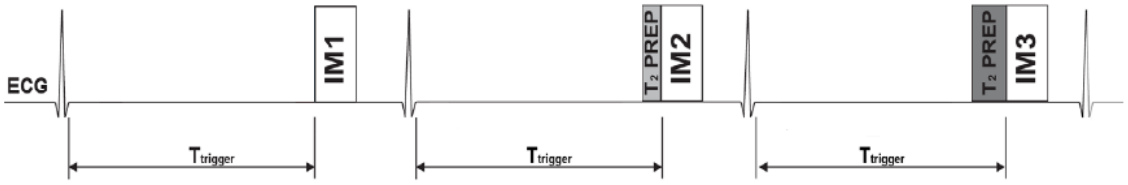

Figure 3.4: Pulse sequence diagram for the T2 mapping sequence. The non-T2prepared acquisition is represented in the beginning.

The respiratory navigators were added as close as possible to the image acquisition to ensure signal similarity across the volumes (Figure 3.5). The same navigator template is used for detecting the motion across all volumes, ensuring co-registration. Also, this approach results in minimization of the time between T2 weighting and imaging leading to more correct contrast. This enables free-breathing acquisitions which allow high-resolution, multivolume 3D scans with whole heart coverage.

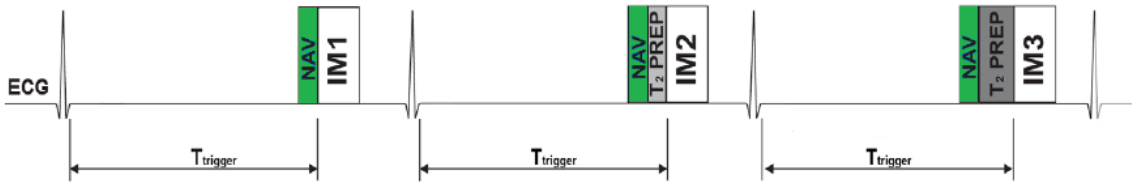

Figure 3.5: Pulse sequence diagram for the free breathing T2 mapping sequence. Each volume is respiratory navigator gated, ensuring coregistered images. An identical navigator template is performed for detection of motion across all volumes, ensuring coregistration. If a given heartbeat is rejected due to respiratory motion, data are reacquired immediately until an appropriate level of motion is achieved before proceeding to the next volume's data.

The user can choose between two different approaches in order to correct for the respiratory motion. One is the d1D NAV, also known as pencil beam navigator (see Figure 3.6), where the acquired images are only accepted if the diaphragm position is within the acceptance window. Navigator echo tracking of diaphragm position is used to compensate for respiratory motion using a combined strategy of slice position. For gating, an acceptance window of 8 mm is used, empirically chosen as a good balance between imaging efficiency and motion sensitivity. Also an empirical correction factor of 0.6 is used to prospectively correct for residual displacement of the slice in the FH direction.

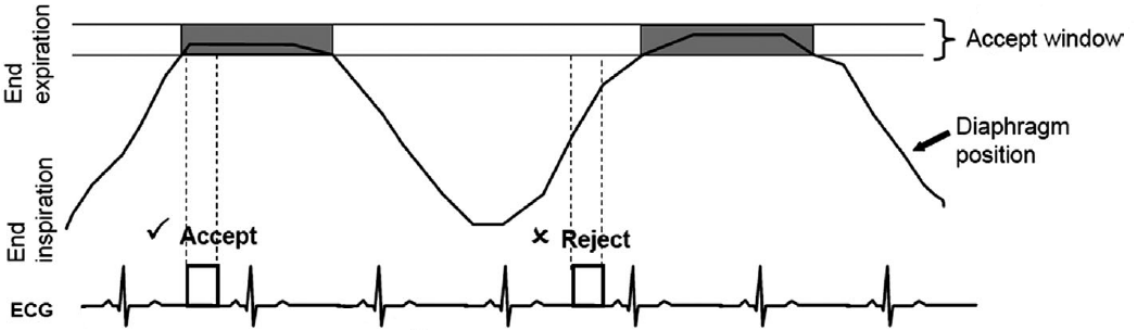

Figure 3.6: Acquisition scheme for pencil beam navigator-gated T2 map. Acquired images are accepted only if the diaphragm position is within the acceptance window.

In the other approach the user can choose the image navigator (iNAV) developed by Henningsson et al. [23]. In this approach a low spatial resolution iNAV is acquired during each cardiac cycle, which will map translational motion. This motion is estimated via image registration for each heartbeat, so called "beat-to-beat" motion correction. In this approach, the motion of the heart is measured directly, allowing translational motion correction to be performed in two or three directions.

The method does not use a respiratory gating window and therefore achieves 100% scan efficiency and a predictable scan time. The operating principles of the iNAV were explained in the previous chapter.

Finally, a saturation (SAT) pulse was introduced and was positioned immediately after the ECG trigger to reset the magnetization at the start of each heartbeat (Figure 3.7). This SAT pulse is a nonselective 90°saturation pulse and removes heart rate and T1 dependency during the scan and allows imaging at every heartbeat. It was applied as soon as possible after the ECG trigger to ensure maximal magnetization recovery before imaging and T_{sat} is held fixed so that the contrast in T1 is maintained.

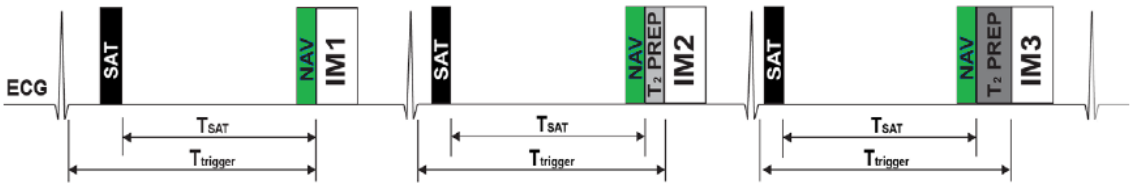

Figure 3.7: Pulse sequence diagram for the free breathing T2 mapping sequence. A SAT pulse was applied at the start of every heartbeat to reduce variations in signal intensities.

To enable in-vivo scanning, the implemented T2 mapping using dynamic scan loop (where the complete k-space of each T2W image is acquired before continuing to the next T2W image, see Figure 3.8a) was extended to segmented/interleaved acquisitions (where the same k-space segment for the different T2W images is acquired in close temporal proximity, see Figure 3.8b) to minimize motion artifacts. However this difference is only visible in human scans.

Data for the differentially T2W volumes was acquired in an interleaved fashion. Interleaving was used to avoid misregistration, which could be present with current single-shot relaxometry techniques and interfere with accurate voxel-by-voxel parametric fitting, or require significant motion correction on a per-frame basis [18]. With the pencil beam navigator approach, if a given heartbeat was rejected due to respiratory motion, data were reacquired immediately until an appropriate level of motion was achieved before proceeding to the next volume's data. The interleaving of the acquisition of the differentially T2W volumes resulted in intrinsic spatial alignment with reduced motion sensitivity and minimized spatial misregistration in the T2W volumes, as any variation in the underlying motion patterns affected all volumes equally [36].

All this sequence and the pulse programming were developed in the PARADISE: Philips Advanced Research And Development Integrated Sequence-programming Environment. This dedicated software from Philips Healthcare is available in the Division of Imaging Science and Biomedical Engineering, King's College London.

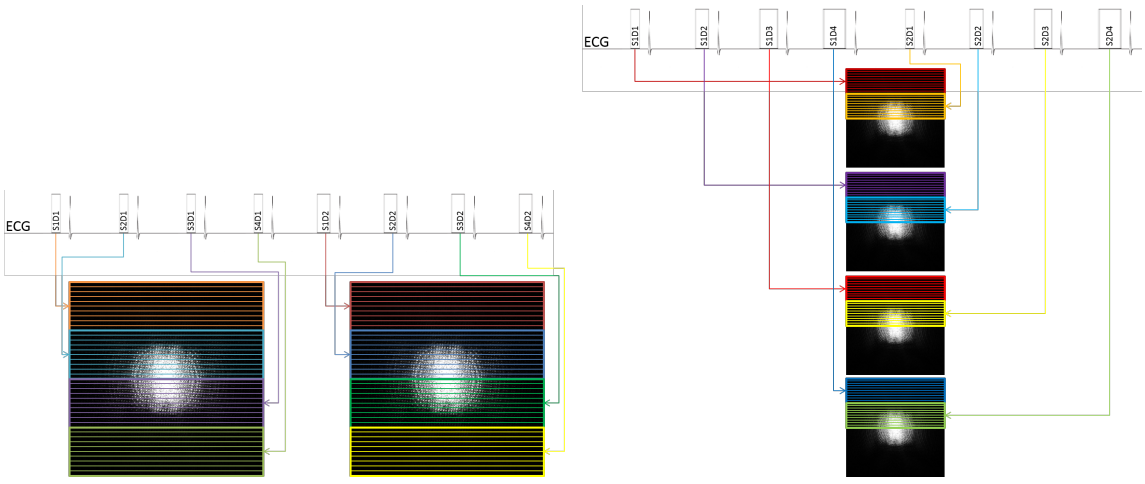

(a) (b)

Figure 3.8: Representation of the difference between the dynamic acquisition (a) and the segmented/interleaved acquisition (B). Each dynamic has a different TE which represents a different k-space segment.

After the acquisition of the images, the T2 maps were generated in MATLAB using a pixel-wise exponential regression method based on a two-parameter equation (Equation 2.3). In order to reduce the computational time, an intensity based threshold was used to remove background pixels from the T2 calculation – only pixels with intensity higher than 100 were included in the fit.

3.2 Phantom Studies

Gel phantom (Figure 3.9) studies were performed to validate the developed sequence. Phantoms (n = 12 tubes) with different T1 and T2 values, were used as the gold truth. These were measured using gold standard spin echo sequences and are duly registered (Table 3.1). The T1 and T2 values vary for each tube because they have different gel densities.

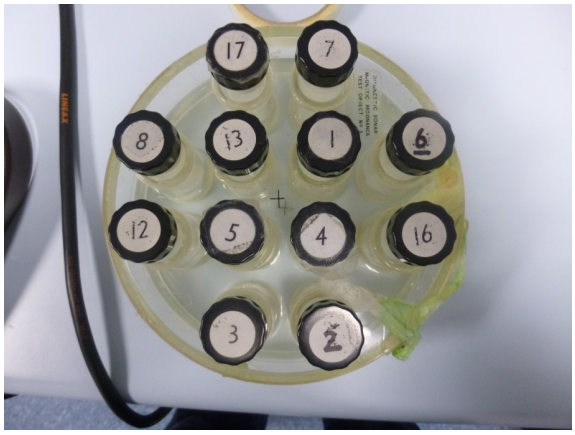

Figure 3.9: Gel phantom (agar/NiC_{l2}) with different T1 (from 200 ms to 1448 ms, at 292K) and T2 values (from 52 ms to 390 ms, at 292K).

Table 3.1: Gel T1 and T2 values for imaging field of 3.00 Tesla. Estimated accuracy = ±3%

	Temperature (K)					
	292	**296**	**300**	**292**	**296**	**300**
Tube No	T1 (ms)			T2 (ms)		
1	200	223	249	52	50	48
2	299	334	372	73	70	67
3	296	331	368	113	111	110
4	463	516	574	53	49	46
5	450	502	559	94	89	85
6	444	496	552	154	151	148
7	604	674	750	95	89	84
8	596	666	741	136	129	124
9	754	841	935	116	109	103
10	745	831	924	157	149	142
11	903	1007	1120	137	128	121
12	1448	1615	1796	390	373	359
13	966	1078	1199	224	212	203
14	1034	1153	1282	167	156	148
15	1160	1293	1437	214	201	191
16	1276	1422	1581	204	190	180
17	1262	1407	1563	184	171	161
18	1415	1576	1750	174	161	151

To determine the accuracy of the developed T2 mapping technique two main tests were performed. In the first one six volumes were imaged with the following T2prep values:

1. 0, 25, 50, 75, 100, 125 ms

2. 0, 30, 60, 90, 120, 150 ms

3. 0, 40, 80, 120, 160, 200 ms

4. 0, 50, 90, 130, 170, 210 ms

5. 0, 50, 90, 130, 170, 210 ms

6. 0, 50, 90, 130, 170, 210 ms

In this study, a large range of TE was used to test the accuracy of the T2 mapping with different combination of values. As the phantoms T2 values vary between 52 and 390 ms, the chosen TEs were inside this range, however the maximum TE chosen was 210 ms because that is the maximum value that can be expected in vivo. Also, the first three values of the set (1) and (2) are the ones that are most likely to be used for the human studies because they are close to the expect T2 value of the myocardium.

In addition to the variation in the TEs, in these sequences the influence of other parameters such as Refocusing Pulses and the impact of Partial Echo in the image acquisition was also studied. In the first 4 sequences the Refocusing Pulses in the T2 prep were set to two and the Partial Echo was enabled. In the 5^{th} and 6^{th} sequence instead of choosing two Refocusing Pulses, the sequences were performed with four Refocusing Pulses. The 5^{th} sequence was performed with partial echo during image acquisition.

A simulated heart rate of 60 bpm was used and imaging was performed using a GRE sequence with TR/TE 4.0/1.23 ms and 5.3/2.6 ms in the last scan. Other imaging parameters were: spatial resolution $1.50 \times 1.50 \times 15.0$ mm^3 reconstructed to $0.59 \times 0.59 \times 15.0$ mm^3.

The second test aimed to explore the sensitivity of the calculated T2 values. A comparison was made between three T2 maps: a 2D T2prep-based with TE of 0, 26 and 46 ms; a 2D T2 map already implemented on the scanner (the T2 fit is made online on the scanner), based on a gradient spin-echo sequence (GraSE, single slice multi-echo breath-hold (BH) scan); and a 3D T2prep-based, where 20 slices were acquired, to see the variations in the SNR. Also this protocol was repeated simulating four different heart rates 60, 70, 80, 90 bpm for middiastole imaging. In total, four T2 maps were used to investigate T2 estimation error as a function of heart rate. The relevant acquisition parameters are summarized in Table 3.2.

In all the phantoms studies, the same ROI was drawn on each phantom on the T2 maps.

Table 3.2: Imaging Parameters for the Phantom Studies

Parameter	**2D T2prep T2**	**3D T2prep T2**	**2D GraSE T2**
Echo Time, ms	0, 26, 46		16.1, 24.2, 32.2, 40.3, 48.3, 56.3, 64.4, 72.5, 80.5
TR, ms	4	5	1000
Flip angle, °	18		90
FOV, mm	320	330	320
Slice Thickness, mm	10	2	10

3.3 Healthy Volunteer Studies

The in-vivo robustness of the T2 determination in the presence of cardiac and respiratory motion was tested in thirteen healthy adult volunteers without known cardiovascular disease (age 29.4 ± 6.2 years, 7 females, 6 males) on a clinical 3T MRI system (Achieva, Philips Healthcare, NL) with a 32-channel phased-array coil. All studies were performed with the same clinical MRI system with subjects placed in the supine position. Each participant provided written informed consent, had no history of coronary artery disease and was not contraindicated for CMR examinations (this was verified via completion of a detailed cardiac MRI questionnaire).

After whole heart shimming and localization, the imaged volume for T2 mapping encompassed the entire heart - as visualized on the localizer scans - and was centered at a left-ventricular level. Images were acquired during diastole. The protocol performed for all the volunteers consisted on:

- 3D T2 prep-based with iNAV correction (Figure 3.10)
- 3D T2 prep-based with pencil beam navigator correction (Figure 3.11)
- 2D T2 prep-based with BH (Figure 3.12)
- 2D Gradient Spin-echo with BH (Figure 3.13)

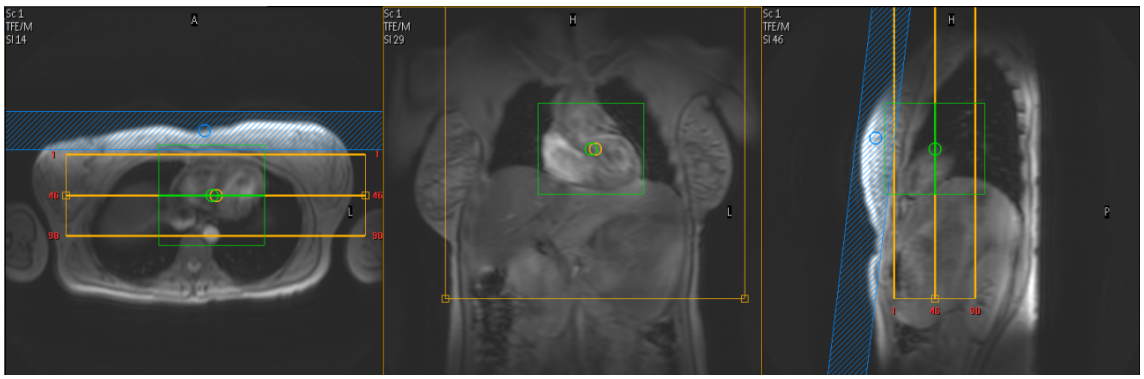

Figure 3.10: Planning acquisition for the 3D T2 prep-based with iNAV correction in a volunteer (volunteer K). 90 slices (yellow box) were acquired to cover the whole heart.

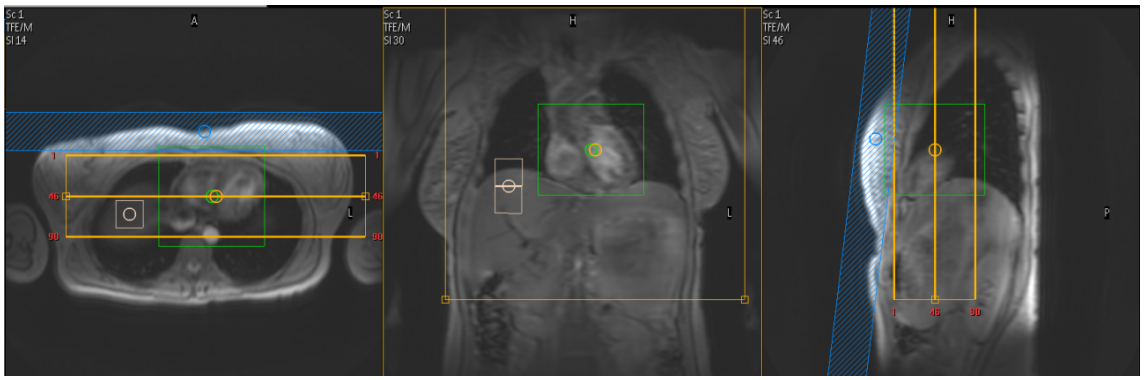

Figure 3.11: Planning acquisition for the 3D T2 prep-based with pencil-beam correction in a volunteer (volunteer K). 90 slices (yellow box) were acquired to cover the whole heart. It is possible to see the navigator placed above the liver (light pink cursor).

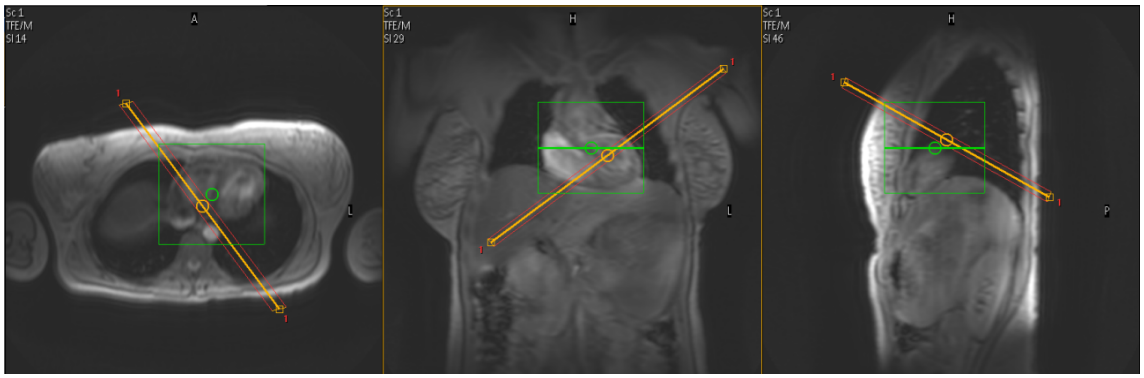

Figure 3.12: Planning acquisition for the 2D T2 prep-based breath-hold (BH) in a volunteer (volunteer K). Only one slice (yellow line) per TE is acquired in the short-axis (SAX) plane.

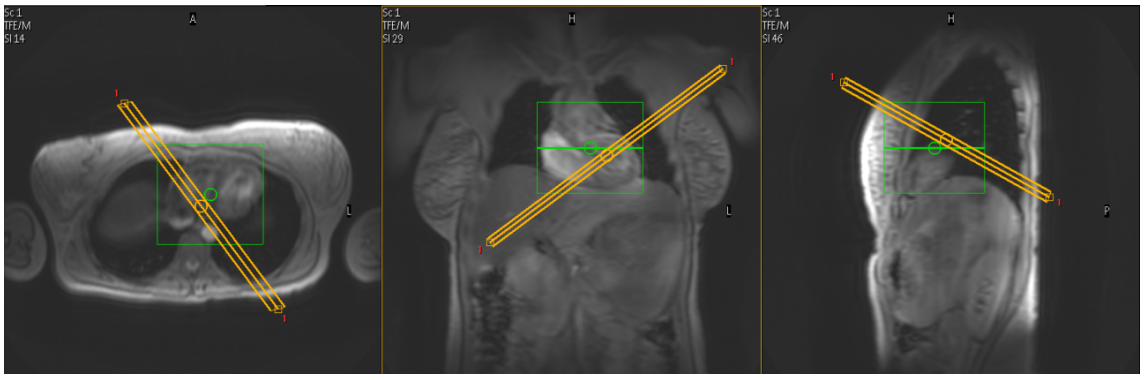

Figure 3.13: Planning acquisition for the 2D T2 gradient spin-echo in a volunteer (volunteer K). Nine slices (yellow lines) per TE were acquired in the SAX plane.

In all the T2 prep studies (2D and 3D) three differently T2W volumes (TE = 0, 26 and 46 ms) were acquired without using any parallel imaging. The 3D sequences were prescribed to cover the whole heart, and 2D sequences were prescribed to match one slice in the heart. The 2D T2 mapping approaches were performed during BH.

As in the human studies there are constrains, like the presence of an irregular heartbeat which may impede the acquisition of the images, the TEs were chosen to be slightly different and readjusted from the ones used in the phantom studies. Based on the results from the phantom studies, on previous studies and on scanner constrains the T2prep TE was determined as 0, 26 and 46 ms.

Different T2 weightings were achieved with adiabatic T2 Prep with different echo times (TE_{T2prep}), including one volume with no T2 Prep and preserved timing. The non-T2-prepared volume (i.e., TE_{T2prep}=0 ms) had the highest SNR and was used to increase image quality. The minimum TET2prep using the standard adiabatic pulses was TE_{T2prep} = 26 ms, because this was the minimum allowed by the scanner. The maximum used TE_{T2prep} 46 ms, which is the estimated value of normal myocardium at 3T [17]. Higher TE_{T2prep} will result in artifacts from residual phase resulting in nonuniform magnetization. This happens because increasing T2prep considerably could reestablish the signal loss artifacts that are characteristic in the BB T2-STIR sequences that are dominant in cardiac imaging, since the T2prep is itself a short spin echo sequence that is intolerant to flow or motion. To avoid signal loss due to motion, both T2prep and imaging should be placed in diastole, which can be difficult for high heart rates or very long TET2prep values.

Because these images are acquired in the transient state of single-shot SSFP immediately after the T2prep pulse, the primary source of contrast is the T2 relaxation time. Thus, the signal in each image represents a different echo time along the T2 decay curve.

In the 2D studies the three SSFP images, each with different T2prep time, were acquired in end-diastole within one BH and the slice was positioned to cover the short-axis (SAX) LV view at mid-ventricular level.

The relevant acquisition parameters are summarized in Table 3.3. The acquisition window in diastole was kept to < 100 ms to minimize cardiac motion [37].

In the 3D studies, to cover the whole heart, between 90 and 110 slices were acquired depending on the size of heart. Although, to avoid imperfect slice profile effects, only three central slices of the T2 map were used for further quantitative analysis (Figure 4.19).

Table 3.3: Imaging Parameters for the Healthy Volunteer Studies

Parameter	3D T2prep iNAV	3D T2prep PB	2D T2prep BH	2D GraSE
Imaging sequence	Gradient echo			Spin echo
Echo Time, ms	0, 26, 46			16.1, 24.2, 32.2, 40.3, 48.3, 56.3, 64.4, 72.5, 80.5
TR/TE, ms	3.3/1.0	4.1/1.2	4.0/1.23	2xRR/40
Temporal resol., ms	73.1±13.6	85.5±11.0	90.8±0.2	100.8±0.2
Flip angle, °	18			90
Acq. voxel size, mm³	2.0×2.0×2.0		1.5×1.5×1.5	1.25×1.28×5.0
Reconst. voxel size, mm³	0.98×0.98×0.98		0.59×0.59×0.59	0.98×0.98×5.0
FOV, mm³	270×220×82			246×226×75
Heart rate, bpm	68±10			
Scan time, s	296±35	308±180	37±4	20±2
Resp. efficiency, %	100	40±12.1	-	-

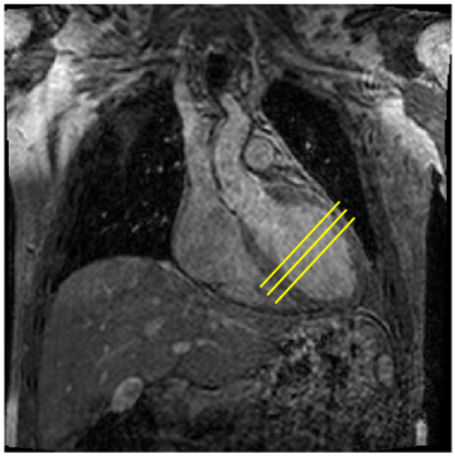

Figure 3.14: Corresponding slice positions of the SAX images along the long axis of the heart.

In the approach with the iNAV correction, the pulse sequence allows for free-breathing acquisitions with 100% scan efficiency, while ECG triggering every heartbeat and adiabatic T2Prep duration TE_{T2prep} = 0, 26, 46 ms lead to a total acquisition time of ∼5 minutes with an isotropic spatial resolution of 1.7 mm^3. In the pencil-beam navigator approach, for respiratory motion suppression during free breathing, a lung-liver respiratory navigator was used. Navigator pulses were placed on the dome of the right hemi-diaphragm. The data was reconstructed as described earlier to generate T2 maps.

In addition, the standard 2D breath-held T2-prepared bSSFP acquisitions were prescribed along representative SAX slices that were matched to three slices centered at the level of mid ventricle within the 3D partitions.

Parametric maps were calculated offline using a two-parameter exponential equation. Two parameters (A_0 and T2) were fit using the following relationship, which assumes that for a given voxel the magnetization at the start of imaging is a function of T1 and T_{SAT}, and an additional exponential term introduced by the T2 decay that occurred during T2prep:

$$S_n = A_0(T_{SAT}, T1)e^{-TE_{T2prep}/T2} \tag{3.1}$$

where S_n is the signal intensity in a given voxel for the n^{th} differentially T2W volume, $A_0(T_{SAT},T1)$ is the signal available right before T2prep and is a function of both T1 and the available time for recovery T_{SAT}, which is a function of heart rate, and TE_{T2prep} is the echo time for the n^{th} T2prep. A_0 assumes perfect saturation, but can also include the residual effects of imperfect saturation. No additional masking was applied to the maps.

The subjects enrolled in the present study were scanned to measure myocardial T2 by drawing a region of interest (ROI) encompassing all myocardium. Three mid-ventricular SAX slices were scanned in each subject. The resulting mean T2 values and mean spatial T2 variation were compared. The coefficient of variation was used as a measure of spatial variation.

Using MATLAB, the LV myocardium was delineated by manually contouring the endocardial and epicardial borders (Figure 3.15. It was ensured that the ROI was definitely within the myocardium and did not include blood or epicardial fat. The trabeculated layer and the epicardial border were left out.

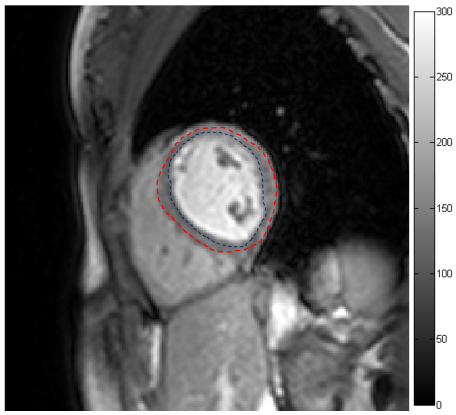

Figure 3.15: Representative myocardial segmentation contours. The red line represents the epicardial border and the blue the endocardial border.

After segmenting the myocardium manually for each one of the tree slices , the mean and coefficient of variation (COV) T2 values of the myocardium determined from images acquired using 2D spin echo, 2D and 3D T2-prepared (proposed) with iNAV and with pencil beam navigator sequences were compared. The mean myocardial T2 values were measured from the segmented myocardium, and the COV of T2 is defined as the ratio of the standard deviation to the mean and it shows the extent of variability in relation to the mean of the population. In MATLAB,

repeated-measurement analysis of variance was performed to examine whether the T2 values were different between different sequences. Finally, the mean T2 value and standard deviation were compared with previous reports from the literature.

For the statistical analysis a box- and whisker plot was performed. The box- and whisker plot illustrates the quartiles in data where each quartile described 25 % of the data. The box illustrates the 2^{nd} and 3^{rd} quartile, which are separated by the median. The whiskers indicate the 1^{st} and 4^{th} quartile and extends to the minimum and the maximum value, respectively. However, the whiskers only extend to the smallest/largest observation when it is not too far from the $2^{nd}/3^{rd}$ quartile (the observation must be within 1.5 $\times$ the interquartile range). Data points that do not fulfil these criteria are displayed as outliers.

To start the statistical analysis, it is necessary to visualize the present data. The normality of the data is further investigated using the Shapiro-Wilks normality test, which tests the null-hypothesis that a sample is normally distributed. When the p-value is less than 0.05, the data is taken to be significantly different, and the null hypothesis is rejected. With a p-value of more than 0.05, the data are taken to be non-significant, and the null hypothesis cannot be rejected. The significance describes how likely it is that a result has occurred by chance, if the null hypothesis is true. The p-value is a measure of the credibility of the null hypothesis.

For the four sequences analysis used in the healthy volunteer studies, the p-value from Shapiro-Wilks normality test was determined to be 3.2613×10^{-8} for the T2 values and 6.6406×10^{-5} for the COV values, so the null hypothesis can be rejected for both cases with a significance level of 0.05. The data is therefore assumed not to be normally distributed. So, for the four sequences analysis a Kruskal-Wallis test was performed in order to determine if the investigated myocardium T2 values calculated based on the four sequences had equal median (med).

The null hypothesis and the alternative hypothesis can be written as:

$H_0 : med_{3DiNAV} = med_{3DPB} = med_{2DBH} = med_{2DGraSE}$

$H_1 : There\ is\ at\ least\ a\ different\ median$

To finalize the analysis, the same Kruskal-Wallis test was done for the three approaches using the T2prep sequence to investigate the differences between them and to see if the iNAV method provided similar results to the pencil beam correction and the 2D T2prep BH.

The new null hypothesis and the alternative hypothesis can be written as:

$H_0 : med_{3DiNAV} = med_{3DPB} = med_{2DBH}$

$H_1 : There\ is\ at\ least\ a\ different\ median$

A similar analysis was carried out for the COV values.

Chapter 4

Results

In this section the results from the studies performed with the phantoms and with the volunteers are presented.

4.1 Phantom Studies

The first study with the phantoms consisted of the evaluation of the accuracy using different TEs. Figures 4.1, 4.3, 4.5, 4.7, 4.9 and 4.11 show the acquired images and the respective TE and Figures 4.2, 4.4, 4.6, 4.8, 4.10 and 4.12 represent the respective T2 maps.

The T2 fitting process took 5668 ± 197 seconds for each map using a 2.67 GHz Intel Core 2 Duo processor, 4GB 2.66GHz and MATLAB.

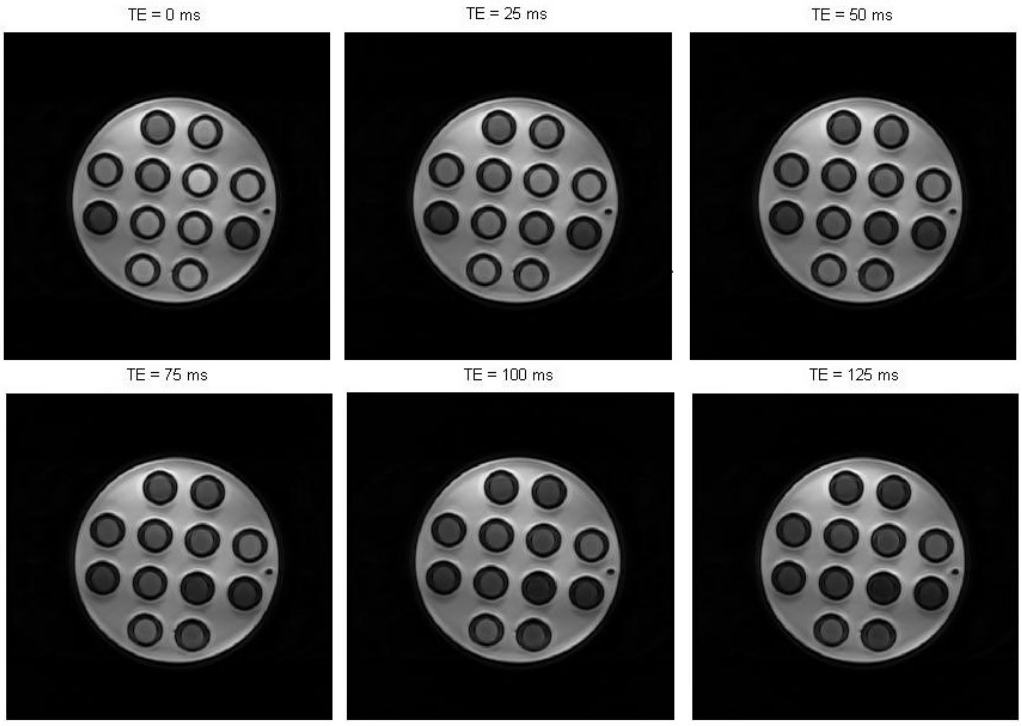

Figure 4.1: Images acquired with the first sequence TE = 0, 25, 50, 75, 100, 125 ms.

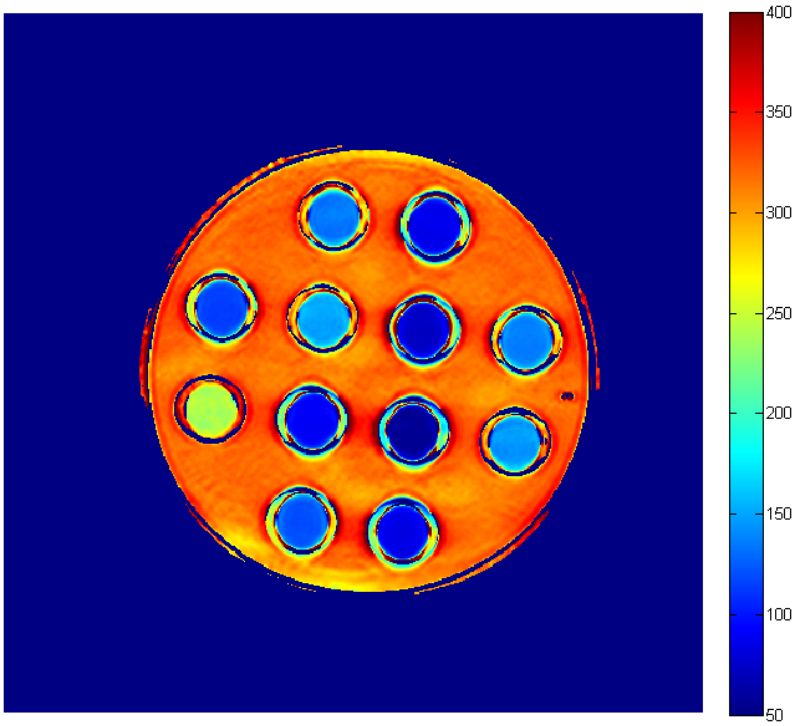

Figure 4.2: T2 map for the first volume of images

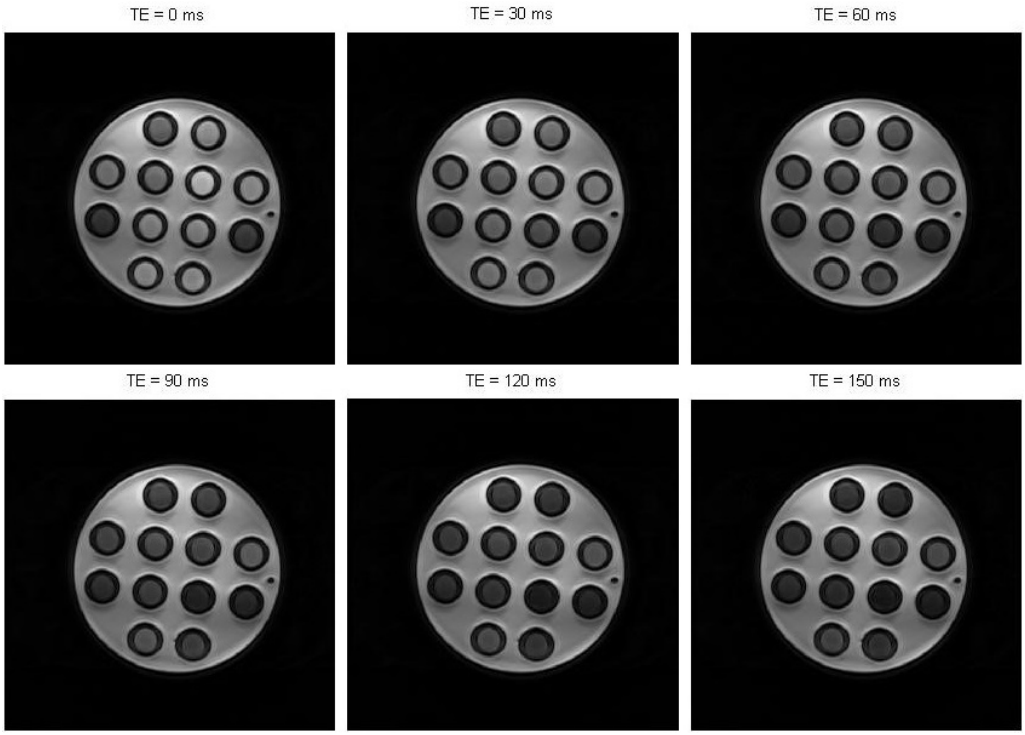

Figure 4.3: Images acquired with the second sequence TE = 0, 30, 60, 90, 120, 150 ms

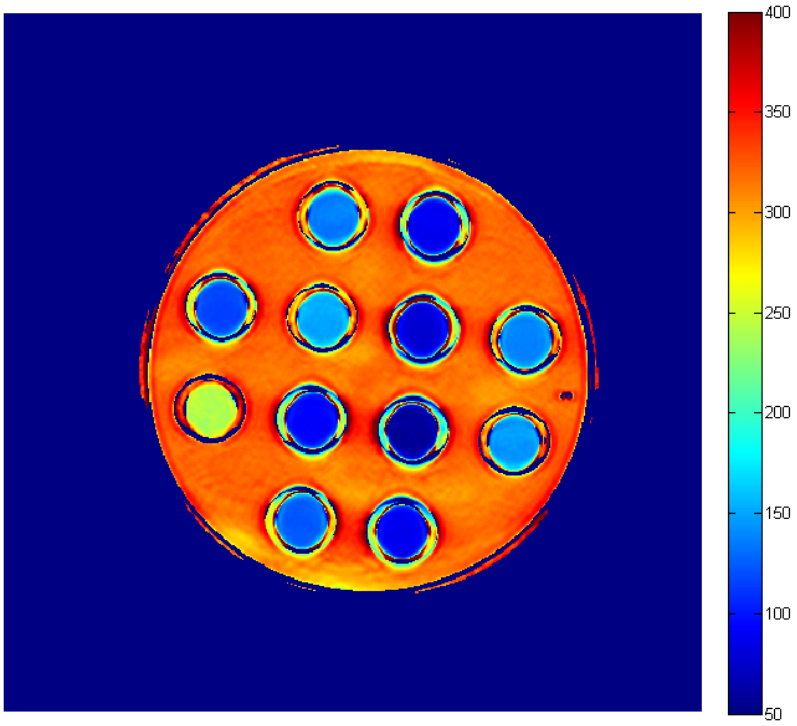

Figure 4.4: T2 map for the second volume of images.

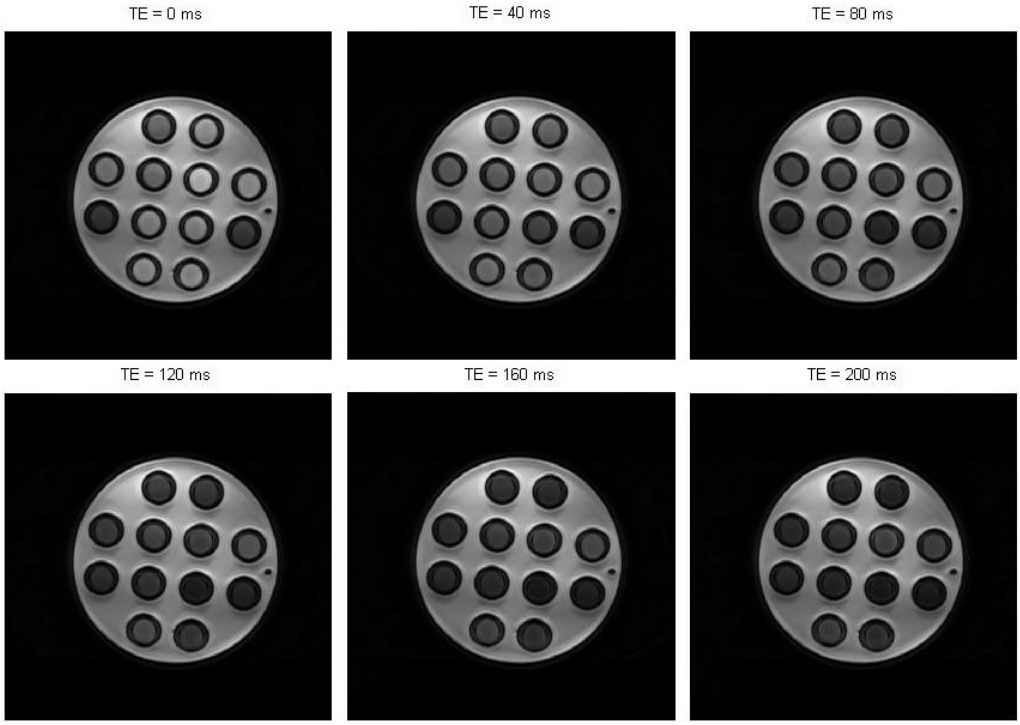

Figure 4.5: Images acquired with the third sequence TE = 0, 40, 80, 120, 160, 200 ms

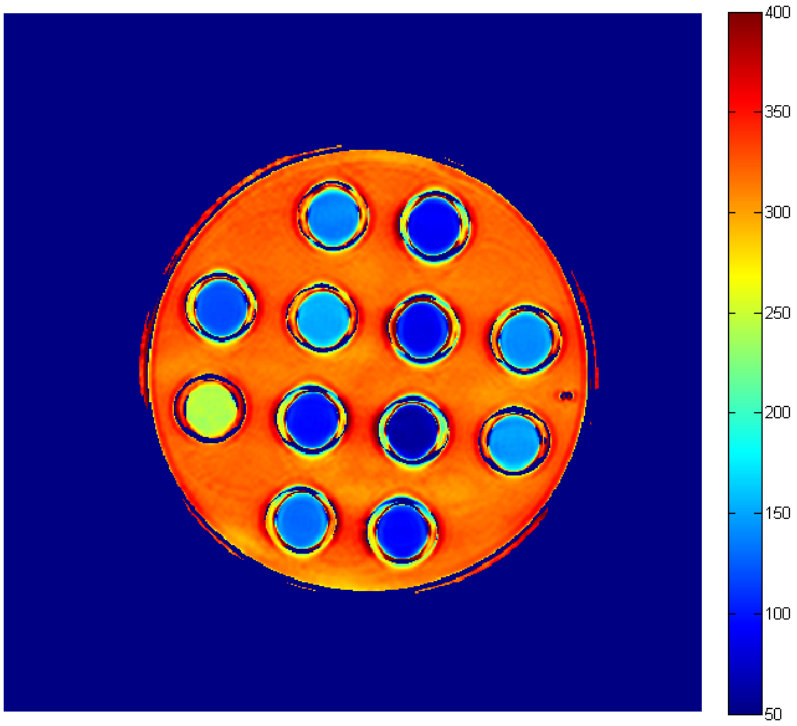

Figure 4.6: T2 map for the third volume of images

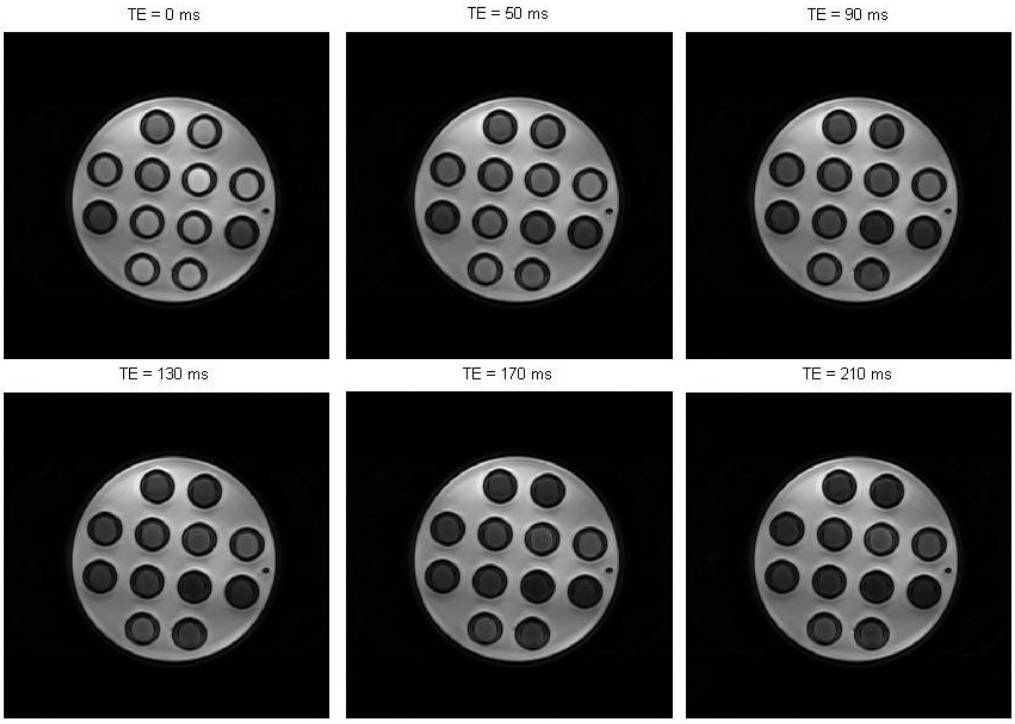

Figure 4.7: Images acquired with the fourth sequence TE = 0, 50, 90, 130, 170, 210 ms

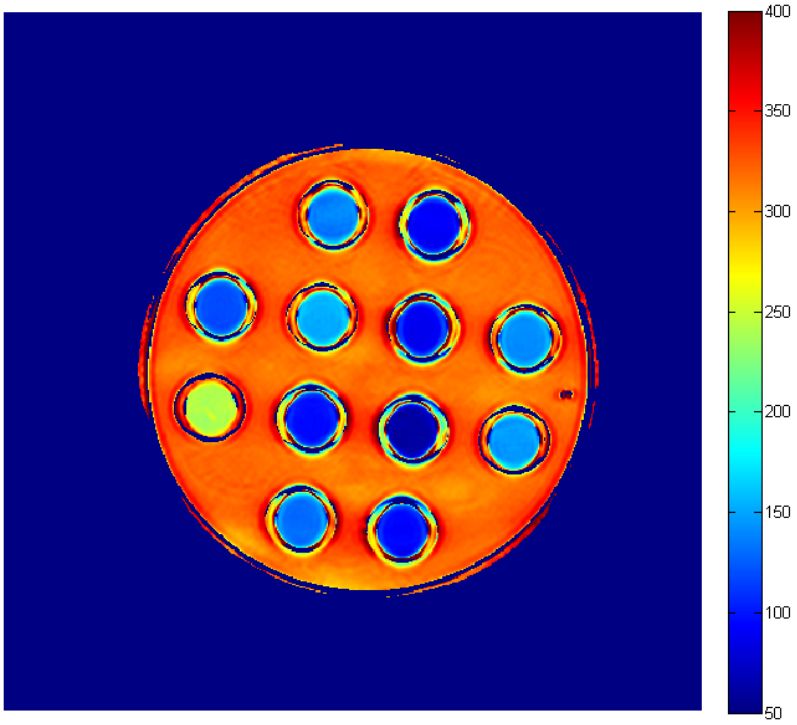

Figure 4.8: T2 map for the fourth volume of images

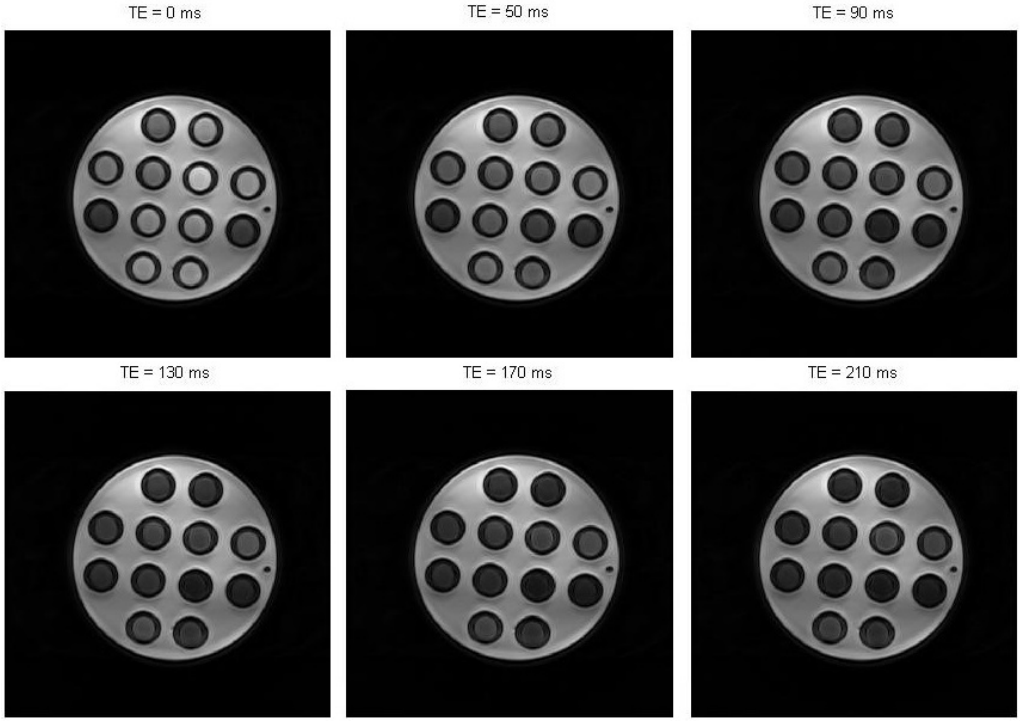

Figure 4.9: Images acquired with the fifth sequence TE = 0, 50, 90, 130, 170, 210 ms and 4 Refocusing Pulses

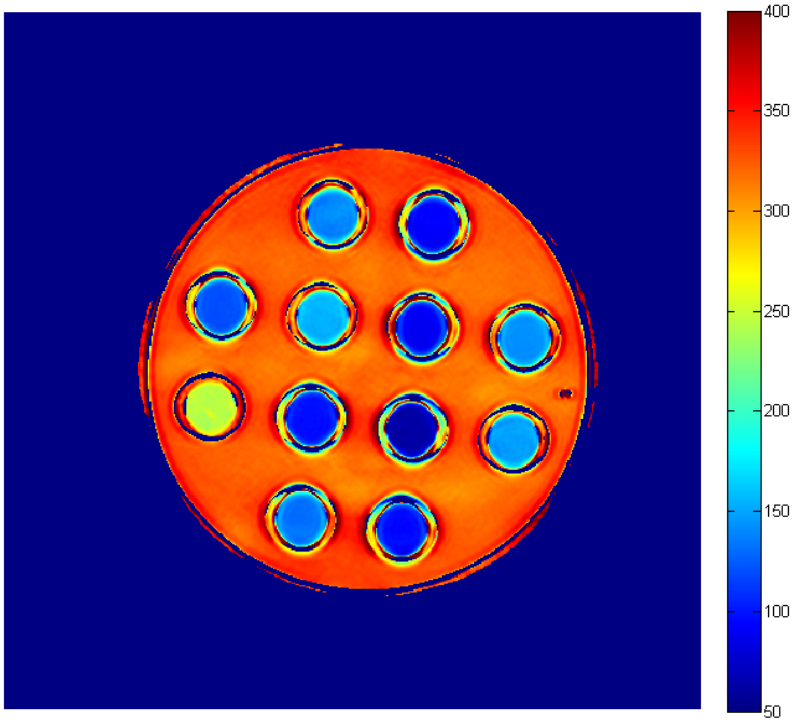

Figure 4.10: T2 map for the fifth volume of images

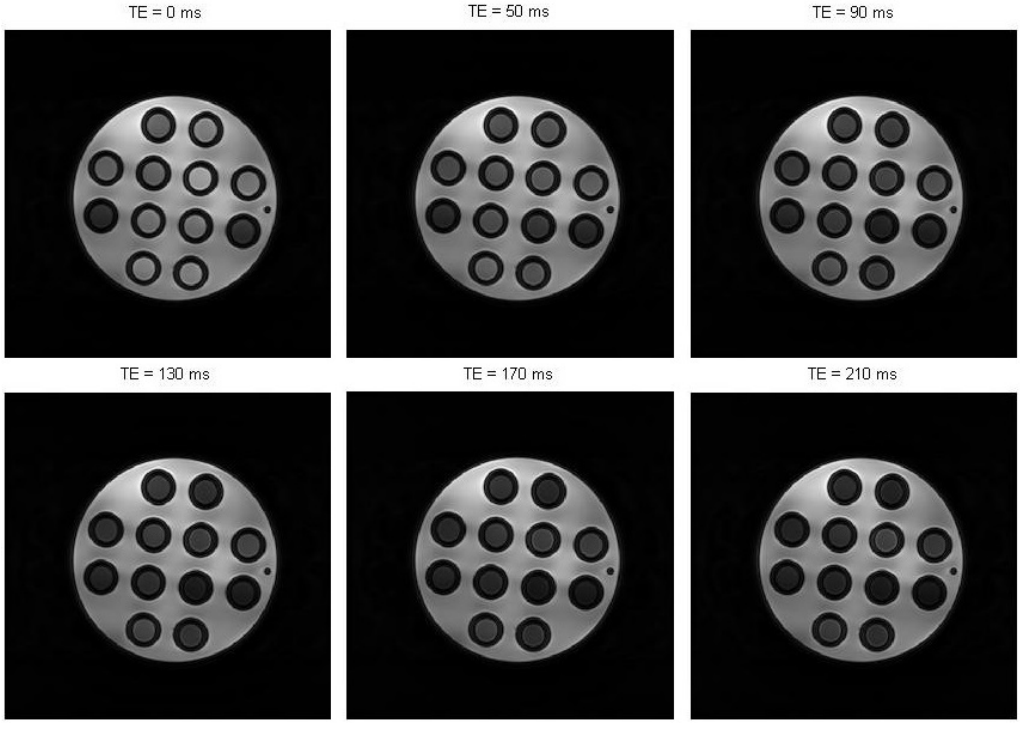

Figure 4.11: Images acquired with the sixth sequence TE = 0, 50, 90, 130, 170, 210 ms and 4 Refocusing Pulses without Partial Echo

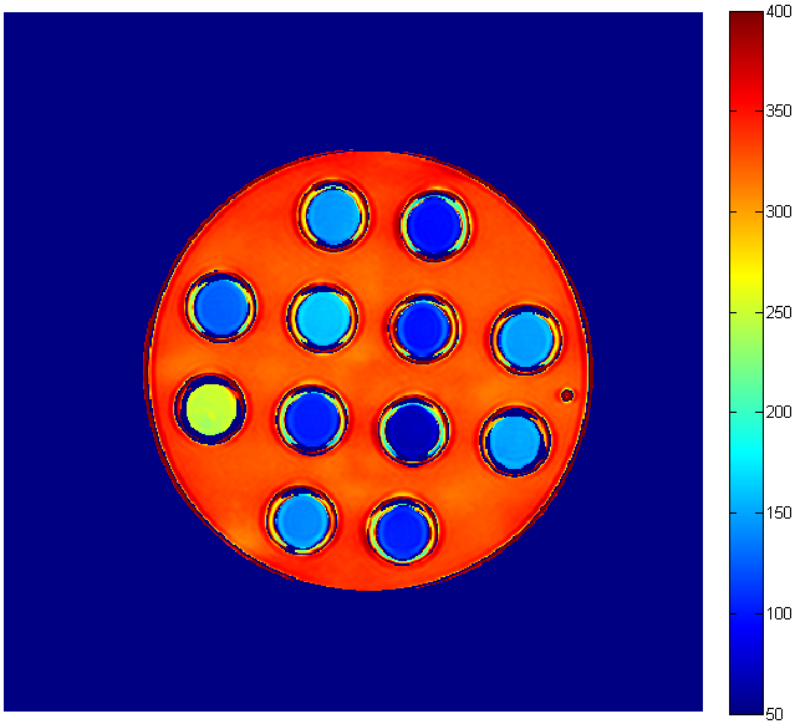

Figure 4.12: T2 map for the sixth volume of images

In order to quantify the T2 values and to compare them with the gold truth values, a plot (Figure 4.13) with the T2 values for each tube was created. To obtain a T2 value from the fitting, an ROI was drawn for each tube and the same ROI was then copied to the other maps.

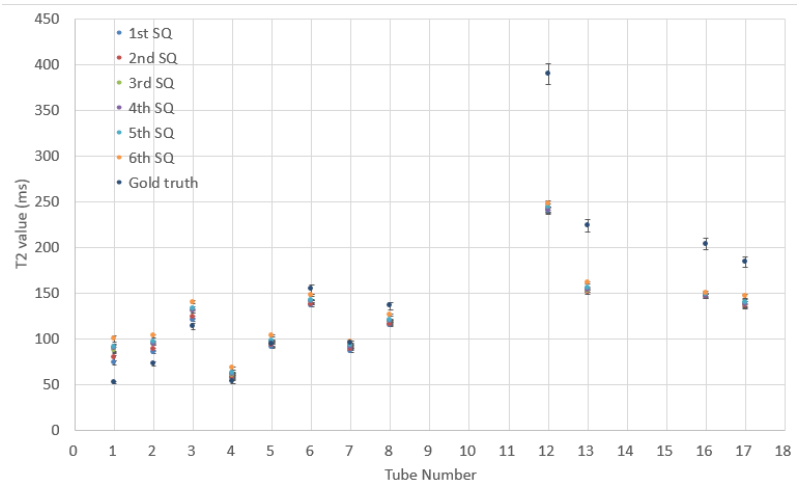

Figure 4.13: T2 values obtained with the T2 mapping sequences and the gold true value for each tube.

Although most of the estimated T2 values were not significantly different between sequences, the sequence which uses longer TE_{T2prep} led to more incorrect estimations for shorter T2 values.

In the second test using the phantoms the influence of the heart rate was studied (Figure 4.14 and Figure 4.15). Also a comparison of the T2 maps derived from the gradient spin-echo (GraSE) approach was performed (Figure 4.16 and Figure 4.17).

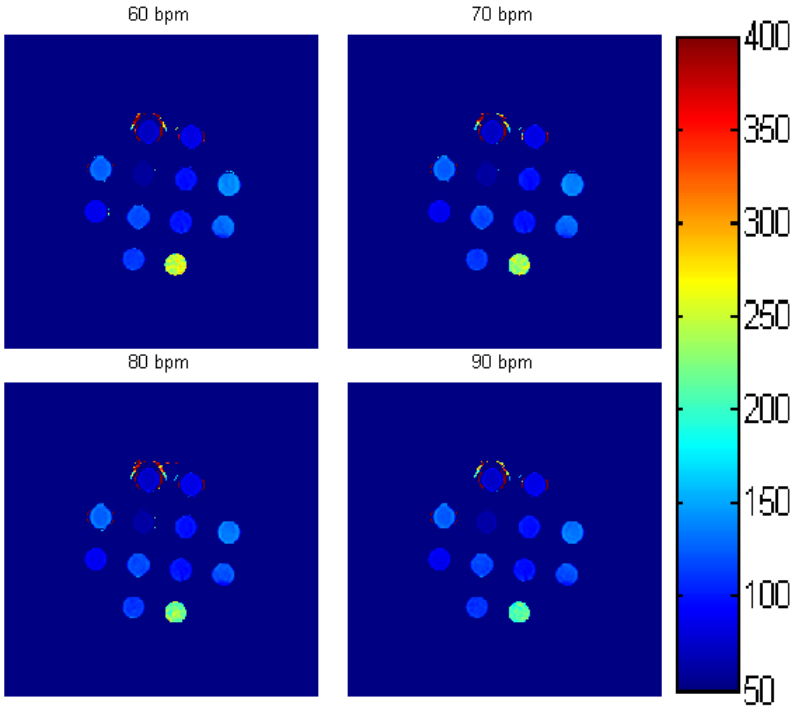

Figure 4.14: T2 maps acquired with the 2D T2prep. The TEs used (0, 26 and 46 ms) were the same for the four scans. The simulated heart rate varied between 60 and 90 bpm.

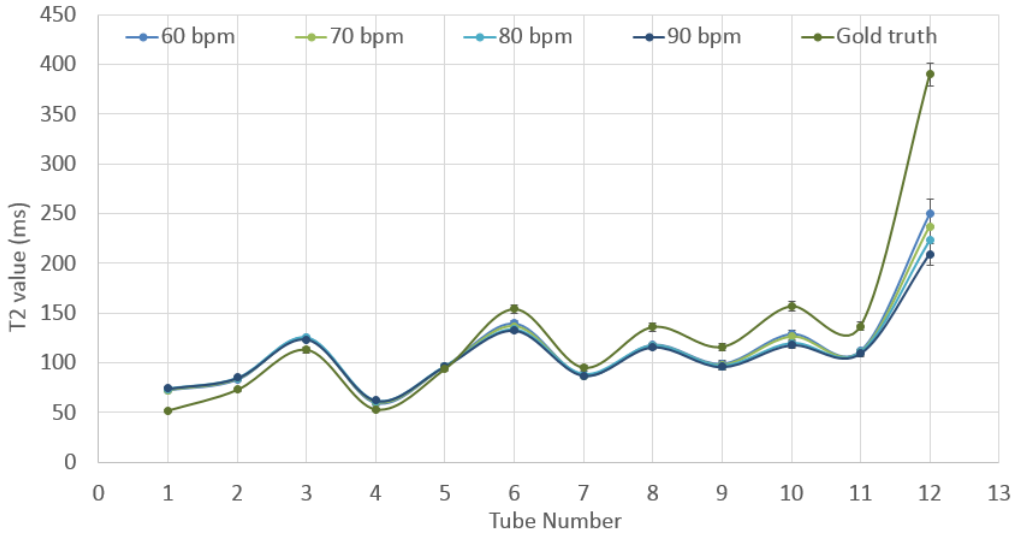

Figure 4.15: Variation of the T2 value estimated for the different tubes of the phantom depending on the simulated heart rate. Each tube has different T2 value (already known). This was calculated using the module of the 2D T2prep.

For longer T2 values (tube 10 and 12) and for long heart rate, the T2 estimation was short. However the image quality was almost the same with different heart rates.

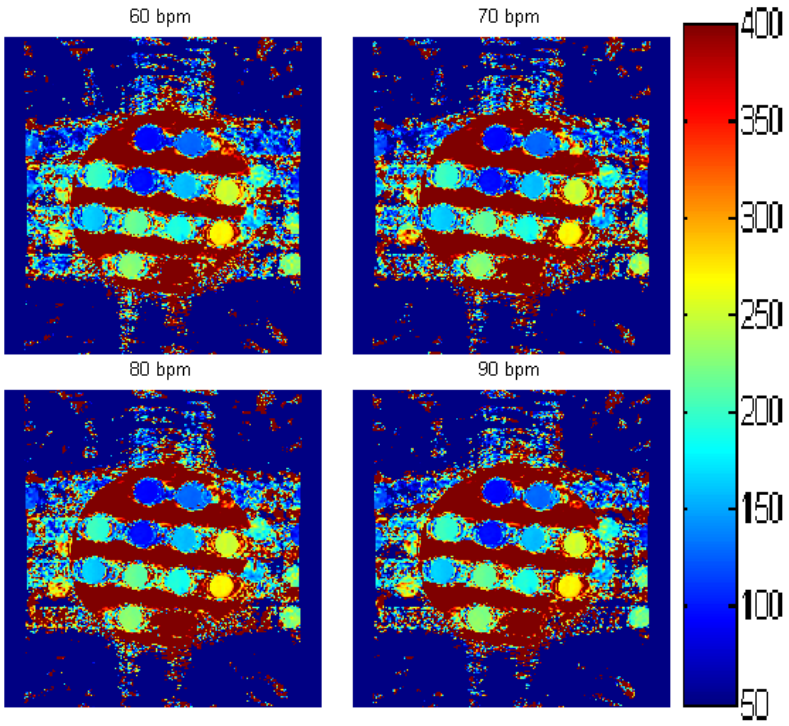

Figure 4.16: T2 maps acquired with the 2D gradient spin-echo. The simulated heart rate varied between 60 and 90 bpm.

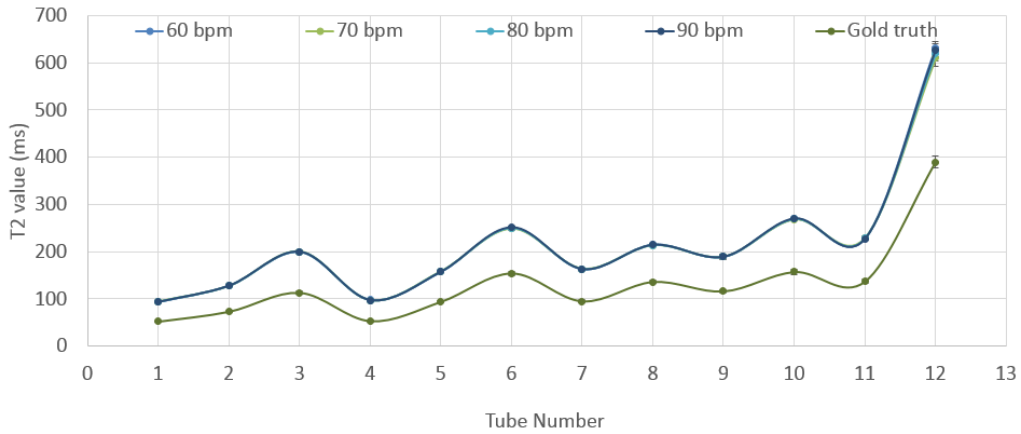

Figure 4.17: Variation of the T2 value estimated for the different tubes of the phantom depending on the simulated heart rate. Each tube has different T2 value (already known). This was calculated using the T2 mapping present in the scanner which is based on a GraSE sequence.

So for both sequences (T2prep and GraSE) the heart rate did not have a strong influence on the available signal. Yet, the GraSE led to an overestimation of all the T2 values while using T2prep resulted in T2 values closer to the gold truth.

Also, an excellent agreement (Figure 4.18) between the T2 maps generated with conventional GraSE and with the T2prep method was found in the phantom study. With a correlation $R^2 = 0.9659$, it was found that T2 computation using the proposed T2-mapping methodology is precise over a large range of T2.

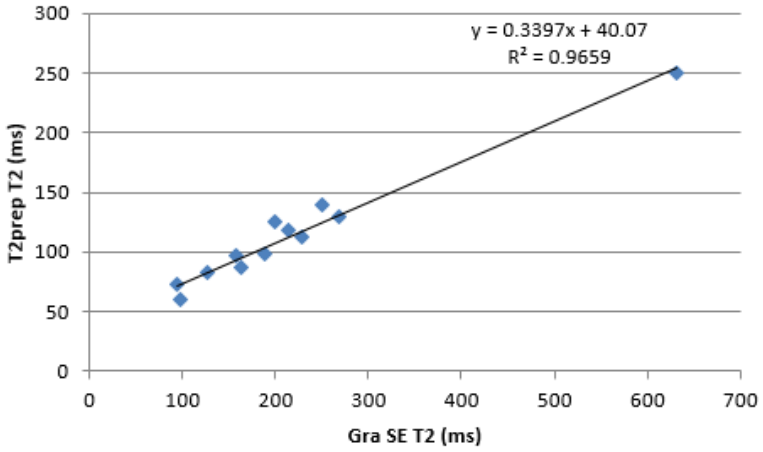

Figure 4.18: Scatter plot of the T2 values of 12 tube phantoms obtained with the 2 T2 mapping techniques. The linear fit resulted in a R^2 of 0.97. GraSE is the T2 mapping technique incorporating gradient spin echo image.

An acquisition in 3D of the T2 maps based on the T2prep was made to see if the performance was similar to the 2D approach. Twenty slices were acquired but only a few slices are shown here as otherwise this section would be overload (Figure 4.19).

Excellent correlations for the T2 values typically observed in myocardium were obtained for all three T2prep combinations, with little residual (R^2>0.99).

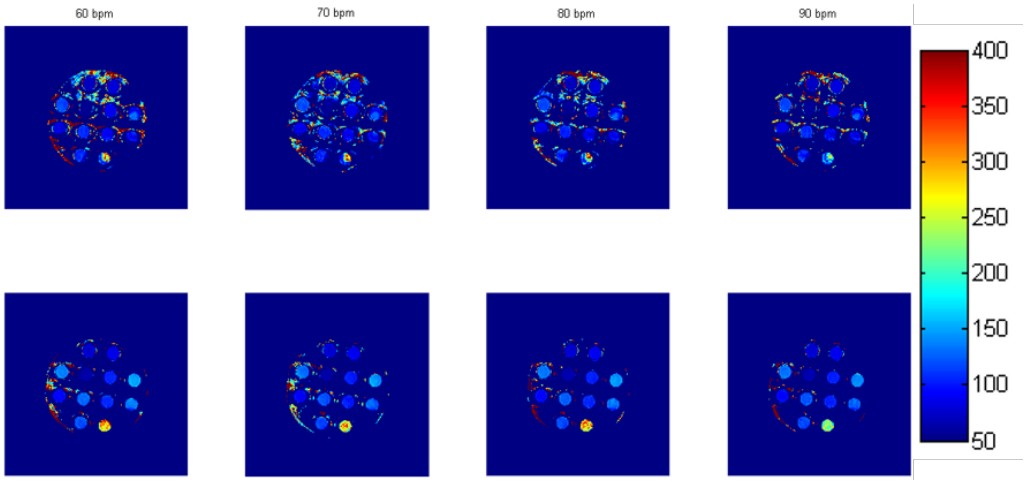

Figure 4.19: Two slices (slice number 5 and 15) of the 3D volume acquired for each heart rate. The showed slices were selected randomly.

Using this 3D approach it was possible to observe that for all the tubes the heart rate led to differences in the T2 value when comparing slices acquired in the same position (Figure 4.20). It was expected that the T2 value of each tube would be homogenous in all the volume of the tube. Although it can be seen (Figure 4.21) that this is not true and the T2 value varies depending on the slice position that is chosen. Also the heart rate led to small changes in the T2 estimation.

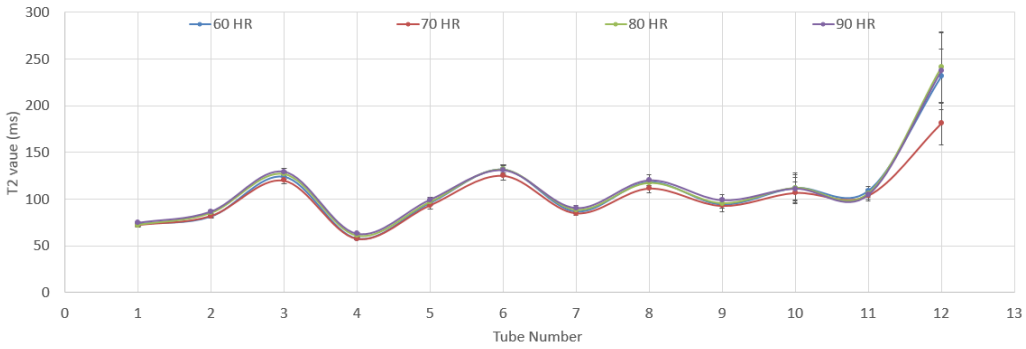

Figure 4.20: Variation of the T2 value as a function of the heartbeat. Only the central slice of the 3D T2prep-based volume is presented.

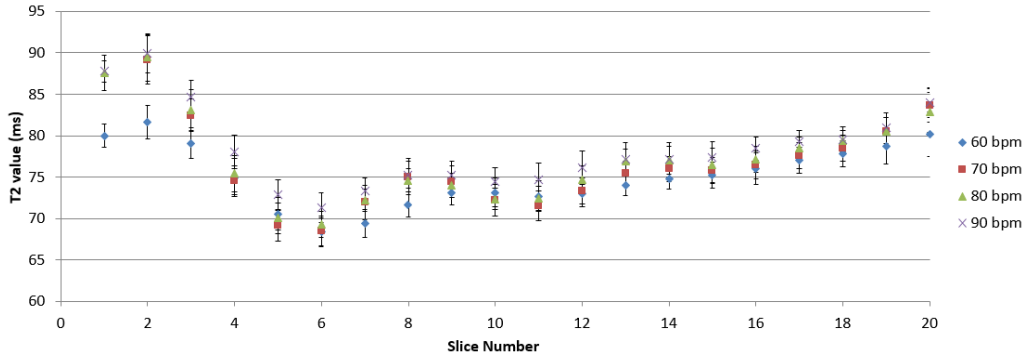

Figure 4.21: Variation of the T2 value along all the slices in one tube (Tube 1) for the four different heart rates.

4.2 Healthy Volunteer Studies

In this part, the results from the human studies are shown. The majority of the optimized protocol was successfully applied in 12 healthy volunteers – except in volunteer B where it was not possible to apply the 3D T2prep with pencil beam and with iNAV, due to the irregular and very unstable heart rate and respiratory cycle.

The proposed 3D free-breathing T2 mapping sequence with pencil beam correction was applied in human subjects successfully with respiratory gating efficiency around 40±12.1%. The average prescribed scan time was 296±35 s and 308±180 s for the three T2-prepared volumes with the iNAV and the pencil beam correction, respectively. Figure 4.22 demonstrates the representative SAX slice of the 3D T2 maps with the two different motion correction (pencil beam and iNAV) and the 2D T2prep-based and the gradient spin-echo (GraSE) from one subject.

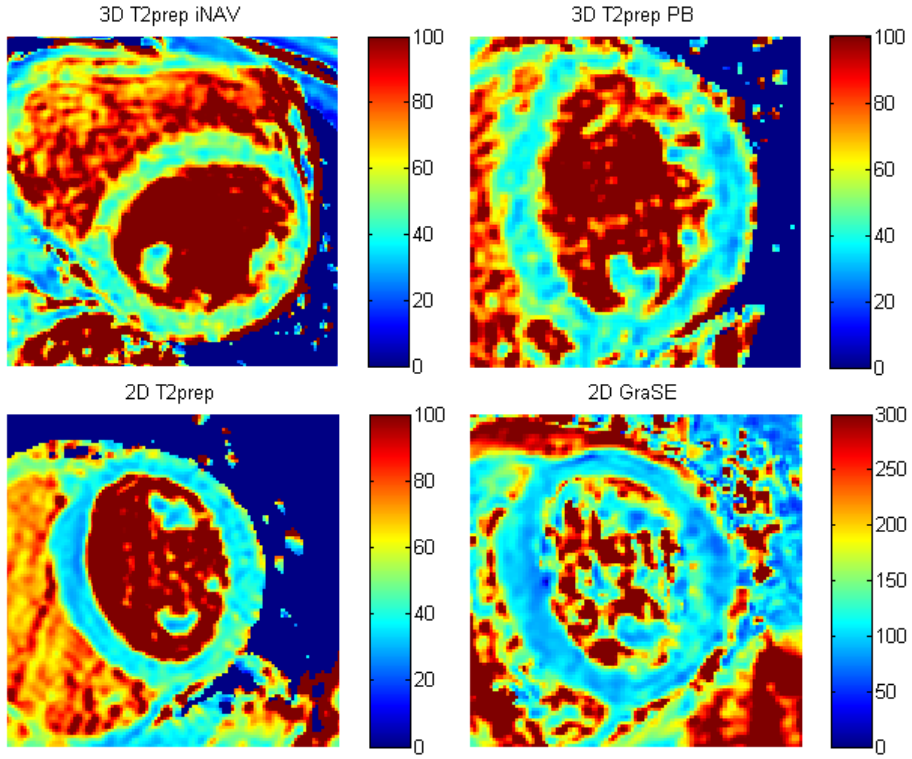

Figure 4.22: T2 maps of one volunteer (volunteer L). Representative T2 maps obtained using 3D T2prep with iNAV and PB (matched to the 2D slice) and 2D T2prep and gradient spin-echo (GraSE) acquisition are shown.

2D T2prep-BH and 3D T2prep-FB with iNAV and with PB maps have comparable image quality, while some artifacts were evident in 2D GraSE-BH maps.

In Figure 4.23 the data for the human scans is summarized in a box- and whisker plot.

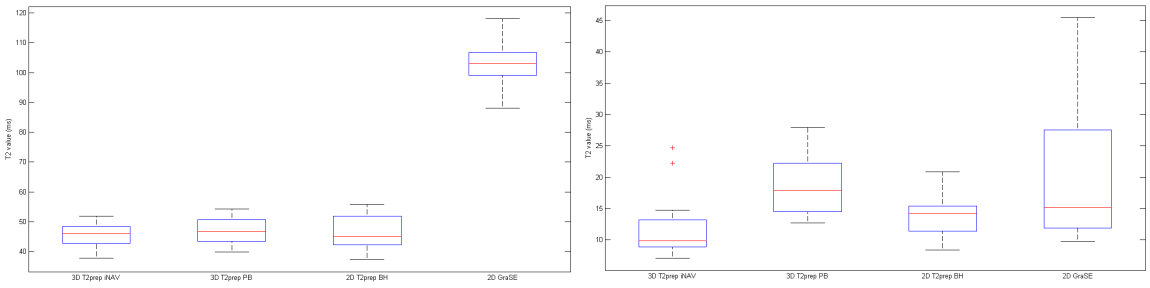

(a) (b)

Figure 4.23: Quantitative measures of mean T2 (a) and coefficient of variation (COV) (b) between 3D T2prep iNAV and PB and 2D T2prep BH and GraSE approaches obtained from healthy volunteers. Across all measures, 3D T2prep iNAV and PB and 2D T2prep BH were not different, but the three approaches were significantly different ($p<0.05$) from 2D GraSE.

As shown in Figure 4.23, the median in the data is similar for 3D T2prep iNAV, 3D T2prep PB and 2D T2prep BH, and the variation in the data from the 3D T2prep iNAV and 2D T2prep BH are similar. Quantitative measures of agreement between the methods are collected in Table 4.1.

Table 4.1: Performance of 3D T2prep PB, 3D T2prep iNAV, 2D T2prep BH and 2D GraSE in Humans.

	Sequence			
Subject	**3D T2prep PB**	**3D T2prep iNAV**	**2D T2prep BH**	**2D GraSE**
Mean T2, ms	47.1 ± 8.9	45.7 ± 5.7	46.1 ± 6.3	102.5 ± 20.5
Mean COV, %	18.9%	12.2%	13.5%	19.7%

The result from Kruskal-Wallis of the four sequences analysis gives a p-value of 6.1933×10^{-6}. The null hypothesis can therefore be rejected, which means that the investigated T2 values cannot be considered to have equal medians. Considering the box- and whisker plot (Figure 4.23) it is easily to understand why the null hypothesis was rejected as the 2D GraSE has a very different range of values in comparison with the other three sequences.

However, the result from Kruskal-Wallis of the three T2prep sequences analysis gives a p-value of 0.6787. The null hypothesis cannot therefore be rejected, and it can be considered that these samples have medians that do not differ significantly.

Similar analysis was made for the COV values. The result from Kruskal-Wallis of the four sequences analysis gives a p-value of 0.0051. So, the null hypothesis can therefore be rejected, and it is assumed that the COV values cannot be considered to have equal medians.

With these results, the same analysis was repeated but this time for just the three T2prep-based sequences. The p-value obtained was 0.0037 so the medians of the COV values are significantly different between the three T2prep-based sequences.

Figure 4.24 represents in detail the T2 values estimated with the T2prep approaches.

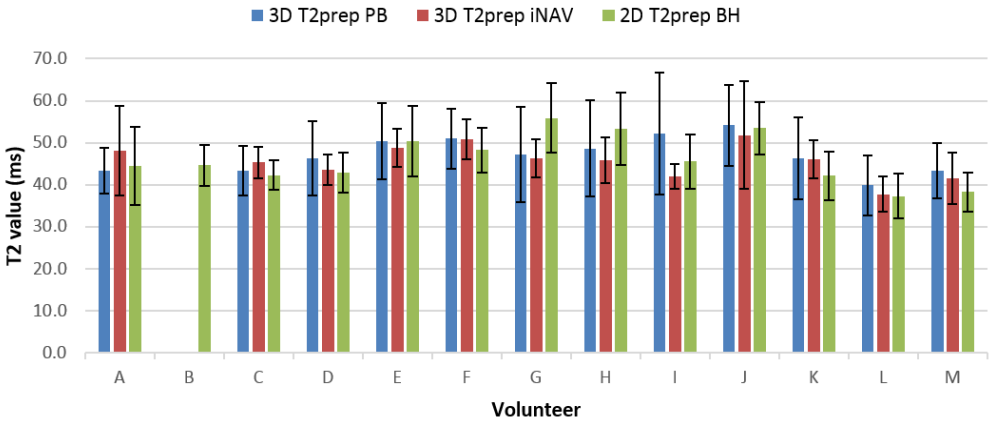

Figure 4.24: Quantitative comparison of the mean T2 values in healthy human subjects from all the three 2D and 3D T2prep approaches tested. There was no statistical difference between the measurements in healthy subjects which used T2prep. The T2 values with $\mu \pm \sigma$ (fitting success rate, %) of the three groups were for 3D with PB: 47.1±8.9 (99.5%), for 3D with iNAV: 45.7±5.7 (99.8%) and for 2D-BH: 46.1±6.3 (99.8%). Some subjects presented increased T2 relative to the rest of the cohort, which may be a reflection of individual variability among subjects in agreement with previous studies [7], [22], [38].

The average T2 values over the whole LV were 47.1±8.9 ms and 45.7±5.7 ms for the pencil beam and iNAV correction, respectively. The corresponding average coefficients of variation (COV) for the two groups were around 19% and 12%, respectively. Note that the T2 maps produced pixel-by-pixel fits with an average R^2 of 0.99±0.01. As already mentioned, no significant difference was found between T2 as measured from iNAV or PB corrected maps. The measured T2 of normal human myocardium was consistent with values reported in the literature (Figure 4.25) [18], [27], [33], [34], [39], [40].

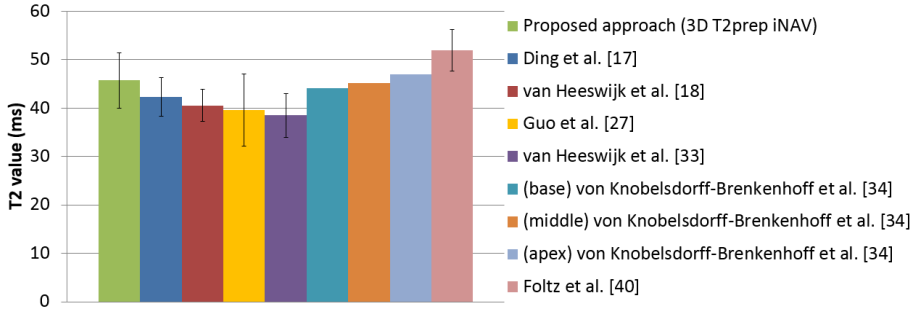

Figure 4.25: T2 values presented in the literature calculated using T2 mapping approaches.

The volunteer study confirmed the duration of the 3D T2prep with iNAV acquisition at 4.56±1.7 min and resulted in an average myocardial T2 value of 45.7±5.7 ms. Which is shorter than with pencil beam (PB) correction, which took 14.2±3 min and resulted in a similar average myocardial T2 value (47.1±8.9 ms). The T2-prepared source images were of high quality, and the resolution allowed for easy reformatting in any desired orientation (Figure 4.26).

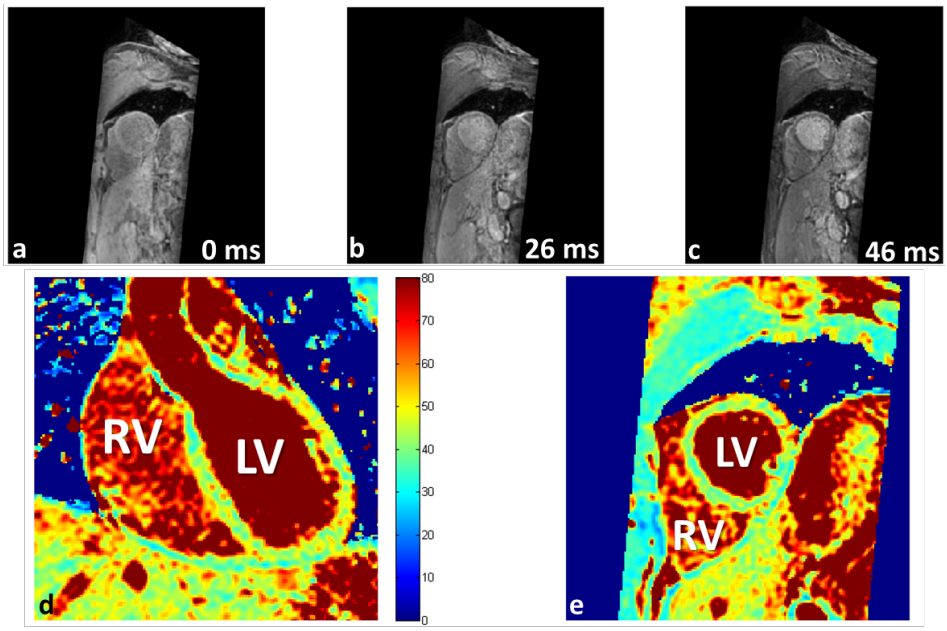

Figure 4.26: 3D T2 mapping in a healthy volunteers (volunteer A) demonstrates a homogeneous T2 distribution. a–c: Three axial source images with different T2prep times and their corresponding T2 map. Despite the relatively low resolution, fine details like the right coronary artery can be identified. d, e: A long-axis and a mid-ventricular SAX slice through the LV show homogenous T2 values throughout the myocardium.

Chapter 5

Discussion

The sensitivity of T2W imaging to myocardial edema was first reported by Higgins [41] over 25 years ago, and several improvements on the original gated T2W spin echo sequence have been made since that time [14], [16], [38], [42]. However, a variety of technical limitations including sensitivity to myocardial motion, surface coil intensity variation, high sub-endocardial signal from static blood, and the subjective nature of image interpretation have restricted the ability to confidently discern true myocardial T2 hyper-intensity with T2W imaging.

This study demonstrates a novel, rapid and practical motion-corrected 3D, free-breathing, T2 mapping technique at 3T featuring heart rate insensitivity and 100% scan efficiency that can be completed within less than 5 min. This quantitative T2 mapping approach addresses these limitations associated with conventional T2W imaging, and may offer a potentially more reliable method for detection of myocardial edema.

The acquisition of multiple differentially T2-weighted (T2W) volumes yielding a voxel-by-voxel T2 map achieved high-resolution, whole heart accurate T2 maps ($2\times2\times2$ mm^3). With this approach no navigator placement or double-oblique anatomical slice orientations is necessary, which allows for minimal planning time and reduced user-interaction in-between scans. Furthermore, this approach not only increases the SNR but also removes any error typically introduced by through-plane motion during BH. Moreover, the spatial resolution and whole heart coverage enable retrospective multiplanar reformatting in any user-selected slice orientation and anatomical level of the heart. Another advantage of this work, is that the integration of volume interleaving instead of sequential volume acquisition (Figure 3.8) guarantees that any change in physiology is spread over all differentially weighted volumes, further guaranteeing accurate intervolume registration and maintaining excellent pixel-wise fitting.

The accuracy of T2 measures from motion-corrected reconstruction was examined in gel phantoms and healthy human volunteers. In phantoms, the proposed T2 mapping sequence achieved excellent accuracy with linear regression $R^2 = 0.99$ making better maps than the standard gradient spin echo. For the healthy human, the results showed that compared with the commonly used T2 mapping approach (2D-BH), 3D T2prep iNav can reliably estimate T2 values of the myocardium at least in healthy myocardium.

Normally the 2D acquisitions that rely on breath-holding constrain not only the achievable spatial and temporal resolutions and coverage, but also risk scan failure in cases with poor subject compliance. Inter-BH movement or any variability in the BH position will lead to discrepancies in measurements and restrict whole heart evaluations. The use of a navigator-gated acquisition removes constrains on image resolutions as demonstrated by the acquisition of whole heart maps with voxel sizes not achievable in a BH or with single-shot imaging. Additionally, motion, variations in heart rate, and T1 dependency are all major factors that impact the accuracy of T2 mapping [4], [18], [25], [26], [33]. Another significant problem recognized even in the first papers on in-vivo T2W imaging of the human heart [43], [44] is sub-endocardial bright signal artifact caused by stagnant blood. Direct quantification of T2 easily distinguishes blood from myocardium [44], within the spatial resolution limits of the sequence. So, the proposed method was designed to minimize the effects of these factors on accuracy.

Also, the 3D T2prep iNAV is expected to be beneficial in patients who cannot tolerate suspension of breathing and in cases where the imaging examination needs to be completed with whole heart coverage within a short period of time. Hence the key features of the proposed approach (free-breathing, full LV coverage and fast acquisitions) are expected to be particularly valuable in the management of chest pain in emergency departments where myocardial edema may be used as a marker of ongoing ischemia [28] and for contrast-free cardiac stress testing using myocardial BOLD MRI [32], [45].

The sensitivity of myocardial signal to motion has been an inherent limitation of techniques such as T2W TSE and STIR imaging where cardiac motion can result in reduced myocardial signal - this problem is often observed in highly mobile basal SAX plane [46]. The T2prep used in this work is non-selective, rendering this technique less sensitive to myocardial signal wash-out than turbo spin echo based methods.

In the present study, the introduction of a SAT prepulse as soon as possible after the QRS complex on the ECG enables efficient scans that utilize every cardiac cycle, removing the need for postprocessing or registration, as all volumes are interleaved and acquired using the same respiratory correction. Existing techniques, which include multiple T1 recovery heartbeats during which no imaging is performed, are susceptible to arrhythmias, and can therefore exhibit T1 dependencies. The “reset” magnetization from every heartbeat provides an ideal baseline for T2 fitting. T1 recovery occurs between the SAT pulse and the imaging impacts on the accuracy of the T2 measurement, which is further reduced by ensuring a constant time between the application of the SAT pulse and the application of the T2prep pulse regardless of the RR interval. Also, in the present study, other positive aspects of using the SAT pulse were offset in part by the expected decrease in SNR of individual volumes. Imaging at 3T using 3D acquisitions provides a high SNR, resulting in robust and stable measurement of T2. However, it is likely that in patients with stable heart rhythms, acquisitions utilizing recovery heartbeats without the use of the SAT preparatory pulse would result in higher SNR efficiency. More work is

required to compare the SNR benefits of either approach.

The step from 1.5T to 3T for CMR is generally desired due to expected gains in signal, which may be exploited for improved spatial and temporal resolution. This potential promises to enable more detailed insights into cardiac tissue in order to facilitate the early detection of myocardial disease. This work was performed at 3T and benefitted from the gain in SNR that was used to achieve higher spatial and temporal resolution. However, the higher field strength also presents challenges due to increased field inhomogeneity and susceptibility artifacts which may affect the image acquisitions. So, the proposed method incorporated the following strategies:

1. A T2prep sequence including adiabatic refocusing pulses made the sequence less affected by $B_1{}^+$ field inhomogeneity [47];

2. A partial echo readout minimized signal loss due to B_0 field inhomogeneity at susceptibility boundaries.

The 3D T2prep iNAV offers robust image quality at 3T because it uses adiabatic T2prep combined with a GRE readout to overcome image artifacts from B1 and B0 inhomogeneities at 3T. Although bSSFP readouts can provide significant SNR benefits over GRE, previous studies have shown insignificant differences in myocardial T2 between the two readout sequences at 1.5T [19]. Nonetheless, both readout schemes have their limitations in extreme cases: GRE acquisitions can suffer from lower SNR and have less homogenous signal in large patients, and bSSFP readouts are prone to unavoidable banding artifacts.

In the present study, the maximum TE_{T2prep} used was 46 ms in vivo. Other studies generally have used between 45 and 60 ms as a maximum value [4], [17], [18], [28]. Although longer TE_{T2prep} values lead to more T2-weighting with more signal loss, they also permit more accurate measurement of longer T2 values in vivo. However, using T2prep risks additional like signal loss due to imperfections in refocusing, including those that result from motion. In fact, increasing T2prep significantly could reintroduce the signal loss artifacts (that are typical in sequences prevalent in cardiac imaging like the BB T2-STIR), since the T2prep is itself a short spin echo sequence that is intolerant to motion. To avoid signal loss due to motion, both T2prep and imaging should be placed in diastole, which can be difficult for high heart rates or for very long TET2prep values.

Although the benefits of fast, free-breathing T2 mapping of the whole LV over the conventional multiple BH T2 mapping are clear, it is useful to contrast the proposed approach against previously proposed 3D T2 mapping approaches. Whereas navigator-gated methods have shown low imaging efficiency and residual motion artifacts, different methods have been proposed to correct for respiratory motion and accelerate acquisition [18], [33]. In particular, the development by van Heeswijk et al. [18] has markedly reduced acquisition time; however, because their T2 mapping approach was found upon 3D high-resolution isotropic imaging, acquisition time

continued to be near 20 min, which imposes limitations on its use for the aforementioned time-sensitive applications.

Generally, myocardial T2 reported in the literature varies substantially, ranging from about 50 ms to 58 ms at 1.5T [4]. The heterogeneity of data underlines that the measured T2 relaxation time is very sensitive to cofactors and emphasizes the need to generate reference values specific for each technique and imaging setting.

However, myocardial T2 reported in the present work was found to be lower versus a mean T2 = 52.2 ms reported for T2 prepared SSFP imaging at 1.5T [4]. Possible explanations are:

a) Differences in the pulse sequence design,

b) Differences in the spatial resolution, with lower resolution being associated with more partial volume and potentially higher T2 values,

c) T1 relaxation effects due to higher T1 values at 3T versus 1.5T.

5.1 Phantoms Studies

In the first study it was possible to verify that both images (Figure 4.1 - Figure 4.11) and the T2 maps (Figure 4.2 - Figure 4.12) are consistent with the expected.

It was found that for T2 values lower than 160 ms, the range of TE values chosen in this study led to good agreement between the calculated and gold truth T2 values. However for higher T2 values, the T2 calculated was lower than expected. This can be explained by the fact that the longest used TE was 210 ms which, in some cases, is lower than the expected value and thus is insufficient to perform the fit properly. As in the human healthy myocardium no high values are expected (the maximum should be below 100 ms) no further studies were performed to test the accuracy.

The accuracy was confirmed in the phantom study where the values obtained with the proposed 3D T2 mapping technique were consistent with those from the gold-standard spin-echo T2 maps (Figure 4.18). The high spatial homogeneity and low standard deviation of the T2 values of $\sim$5% further demonstrated the robustness of the pulse sequence in vitro.

The comparison between the six TE_{T2prep} combinations showed there were only slight differences in the values of their regression intercepts and regression slopes. The comparable performance observed when using measurements derived from six TE_{T2prep} values implies that three volumes may be sufficient for the desired T2 measurement accuracy for the signal-to-noise levels achieved in this setting and are therefore suitable for use in in vivo acquisitions.

In the second study, heart rate was found to significantly influence T2 measurements ($p<0.0001$). Higher heart rates were associated with a reduction in T2 values. The phantom experiments confirmed that the use of the optimized 3T methodology resulted in accurate T2 measurements relative to conventional spin-echo measurements as the gold standard.

The association of heart rate and T2 relaxation time is still under discussion. Giri et al. reported that the variability between healthy subjects was unrelated to heart rate. Other studies reported lower T2 values in patients with higher heart rate [5]. This may be attributed to the hypothesis that higher heart rates induce pronounced T1 relaxation effects caused by incomplete T1 relaxation, which may affect T2 mapping using SSFP-based approaches. This finding is very relevant for clinical practice as subtle T2 increases may disappear in acutely ill patients with higher heart rates.

5.2 Healthy Volunteer Studies

The methodology was further characterized in an in vivo healthy volunteer study where its effectiveness and reproducibility were evaluated. The T2 maps T2prep-based displayed consistent image quality in all cases, whereas the quality of GraSE images varied significantly (Figure 4.22).

The T2 values measured under heathy conditions in this study were comparable to the values previously reported in humans and reported in the literature [27]. Specifically, the T2 value of healthy myocardium was found to be 45.7 ± 5.7 ms. The favorable comparisons between the results of this work and those reported in the literature further confirm that 3D T2prep iNAV is a reliable method for measuring myocardial T2 under healthy conditions. The pixel-wise T2 found in this study is higher than some previously reported values [4], possibly because contours, drawn to cover the entire myocardium, included border pixels with partial-volume effects. Additionally, the misregistered pixels varied over a very wide range. In a quantitative approach, the resulting outlier pixels could potentially be flagged as pathologic tissue. A clinical study [48] defined a region as pathologic if 10 or more connected pixels had abnormal T2W signal. With this as a reference, the proposed technique performed well, because most of the outlier pixels were scattered around the borders, without forming a connected region.

Also, the T2 values in the healthy volunteers were consistent with those previously reported at 3T even when obtained with a 2D technique, on a 1.5T scanner or using BH approaches, and have a similar standard deviation of $\sim$8% [33]. Gradients in measured T2 values were observed in both the base to apex direction and around the circumference from the anterior to the inferior SAX segments. As the anterior and posterior parts of the heart are positioned differently within the RF-excitation body coil, there is a residual decreasing gradient of effective RF excitation angles from the anterior to the posterior direction. Such a gradient in effective RF excitation angle, therefore, results in a minor gradient of T2 values in the anterior-inferior direction.

Future studies could, for example, try to correct for this effect by incorporating maps of the effective RF excitation angle. Simultaneously, different distances from the receive coils might result in decreased SNR in the inferior segments, which could in turn result in a T2 overestimation. However, given that the lowest myocardial SNR of the T2prep = 46 ms images is on the order of ∼10, this should account for only about 1 ms of overestimation. Differences in instantaneous regional myocardial perfusion (and thus oxygenation) between the base and apex may furthermore lead to the observed variations in the apex-base direction. Other studies [4], [34] also observed variations in the apex-base directions. These differences are most likely due to more obvious partial volume effects resulting from bigger voxels, an effect that is more pronounced in the apical regions of the heart. However, as these studies used 2D breath-held T2 mapping, a direct comparison may not be straightforward.

Another challenge is the high inter-subject variability of T2 mapping, given that the difference in T2 between healthy and injured myocardium has been reported to be relatively small, e.g. 13 ms/11 ms between infarct core/myocarditis and remote myocardium [5], [28]. This range of T2 value differences may occur due to slight changes related to B_0 and B_1 inhomogeneitis, the relative accuracy of the fitting procedure, coil placement, among others. Furthermore, and consistent with prior reports that established T2 mapping at lower field strength, only 3 points were used for the mono-exponential 2-parameter fit for the T2 determination in this study. Although more points may result in an improved accuracy and robustness of the procedure, this remains to be investigated and has to be carefully balanced versus an increase in scanning time.

5.3 Limitations

Despite this work have achieved very promising results, it has some limitations. First, although healthy volunteers have been used to show that 3D T2prep iNAV can yield values of T2 similar to those obtained with 2D-BH, the sample size of the study was limited. Given that the primary purpose of this study was to validate the iNAV correction for T2 mapping, patients were not recruited as the myocardial T2 variability in patients would likely have confounded the investigation of variability due to misregistration. Additional studies are required to assess the robustness of the method under various physiological conditions, particularly in human subjects with disease. The effects of variable myocardial signal, as may be found in pathologies could be investigated.

Second, based on the monoexponential model, three TE are the minimum requirement for a least-squares linear regression fitting of the logarithmically transformed data. Although additional TE may improve robustness of T2 fits [49], extra acquisition time associated with a greater number of TEs can extend the study time beyond the demands of the key applications outlined earlier. Based on the results of the current study and those of others [4], [5], [29], [33], [34], three TE provide a good trade-off between imaging speed and fidelity of myocardial T2 fits under conditions of health and disease.

To map the T2 of the myocardium, the longest TE was set to be 46 ms to achieve a reasonably dynamic range in signal intensities and still have sufficient sensitivity to accurately identify the remote myocardium (T2 of ∼40 ms). However since affected areas tends to have a T2 of ∼60 ms, it should probably be better to consider an increase to ∼55 ms. Also, the shortest TE_{T2prep} used in this work was 26 ms, which is limited by the current system and the choice of standard adiabatic pulses for refocusing. The performance of the sequence could likely be improved by using shorter adiabatic pulses (at the expense of $B_1{}^+$ homogeneity) that would in turn permit better distribution of the TE_{T2prep} values and better sampling of the T2 decay curve of short T2 species. Further exploration is needed.

Third, it is assumed that the prescribed slice positions for 2D and 3D acquisition were the same, which may not be the case. In addition, given that 2D slice thickness and 3D partitions is similar (2 mm), it is anticipated that any contributions from potential differences would be small. This work reported T2 values only for a midventricular slice. By averaging T2 values over the whole heart, focal T2 deviations may be overlooked:

a) As hematocrit was not measured in this study, its effect on T2 relaxation time could not be assessed.

b) Whereas observer variability to assess T2 relaxation times was low, the interscan variability was not assessed and deserves further investigation.

The nonselective SAT prepulse used in this study was not insensitive to $B_1{}^+$ field inhomogeneity, which could result in compromised T2 measurement sensitivity to arrhythmias via residual unsuppressed signal [50]. Similarly, the rectangular nonselective 90° tip up/down pulses used as part of T2prep could lead to imperfect magnetization preparation and errors in T2 measurement, since the non-T2-prepared volume is imaged with full magnetization. The use of a surface coil can also be considered as a limitation in the study because the inhomogeneous coil sensitivity profile reduces sensitivity for inferolateral infarction, whereas it may overestimate anteroseptal edema. Variability in myocardial signal in T2W imaging can also result from surface coil intensity inhomogeneity, another important factor limiting the applicability of myocardial edema imaging.

Another potential limitation of iNAV 3D cardiac T2 mapping is its duration. The 3D T2 maps presented here were calculated from fully sampled acquisitions of three T2W volumes. Although 3D acquisitions require significantly longer scan times which are not amenable to single-shot acquisitions, k-space segmentation permits much higher temporal and spatial resolution, producing higher-quality parametric maps with low COVs. The averaged prescribed scan time for three volumes corrected with the pencil beam and with iNAV with a field of view of approximately $270\times220\times82$ mm^3 was 14.2 min and 4.56 min, respectively. Although the scan time with iNAV is shorter than previous studies presented in the literature, these scan times can still present a barrier to the use of the proposed technique in a routine

clinical examination. However, no acceleration in the form of parallel imaging was used to facilitate accurate measurement of SNR. A shortening of the scan time could, for example, be achieved by acquiring more lines per heartbeat, partial acquisition schemes, such as k-space weighted image contrast (KWIC) [51] or k-t FOCUSS [52] or the use of compressed sensing. However, the effects of all such scan time shortening techniques on the performance of T2 mapping remain to be more thoroughly investigated. In fact, it would be interesting to test if any of the available 3D subsampling strategies is applicable (e.g., 3D-SENSE or 3D-GRAPPA) [53], [54]. Also, because the multiple volumes acquired are quite similar, there is no reason not to believe that with the current state-of-the-art acceleration strategies, even larger acceleration factors can be achieved using reconstruction techniques that incorporate the parametric maps as final products [55], [56].

However, to avoid potential smoothing artifacts observed in certain accelerated approaches and also to strictly examine the capability of motion correction, no imaging acceleration techniques were considered. Additional studies are needed to examine the limits of imaging acceleration strategies within the constraints of reliable measurements of myocardial T2.

Chapter 6

Conclusion and Future Work

In this work, a novel approach was successfully implemented, tested and characterized providing robust free-breathing accurate 3D T2 maps that are feasible and may be applicable in myocardial assessment in lieu of current clinical BB, T2-weighted techniques. It was also demonstrated an automatic and reliable free-breathing myocardial T2 mapping technique based on single-shot, T2-prepared SSFP with iNAV correction. The proposed whole heart T2 mapping approach allows for 3D characterization within less than 5 min with a high degree of homogeneity and similar accuracy to that of the 2D-BH T2 mapping approach.

The sequence takes advantage of the higher SNR available at 3T. A SAT prepulse is used to decrease sensitivity to heart rate variability and arrhythmias, and volume-interleaved acquisitions remove issues of misregistration between the multiple volumes used in the voxel-wise calculation of T2. Quantitative T2 mapping addresses the well-known problems associated with T2W imaging of the heart. This respiratory 3D technique allows for accurate and robust T2 quantification. The proposed approach yielded accurate estimates of T2 in gel phantoms and myocardial T2 in healthy human volunteers.

The accurate and quantitative nature of 3D T2 mapping makes it a great candidate for future use in in vivo studies to explore the lesion healing process, assess novel therapies, or provide a tool for the assessment of the area at risk and risk stratify a patient post MI. Also, this technique may be well suited for longitudinal studies in patients with suspected or established ischemic heart disease.

Clinical studies are needed to validate the robustness of the proposed approach in patients. Further studies on reproducibility and the pathological evolution of acute injury may be needed to best deploy this quantitative technique.

Bibliography

[1] Karamitsos TD, Francis JM, Myerson S, et al. "The role of cardiovascular magnetic resonance imaging in heart failure.," J Am Coll Cardiol. 2009; 54:1407-1424

[2] M. G. Friedrich, U. Sechtem, J. Schulz-Menger, G. Holmvang, P. Alakija, L. T. Cooper, J. A. White, H. Abdel-Aty, M. Gutberlet, S. Prasad, A. Aletras, J.-P. Laissy, I. Paterson, N. G. Filipchuk, A. Kumar, M. Pauschinger, and P. Liu, "Cardiovascular magnetic resonance in myocarditis: A JACC White Paper.," J. Am. Coll. Cardiol., vol. 53, no. 17, pp. 1475–87, Apr. 2009.

[3] M. Salerno and C. M. Kramer, "Advances in parametric mapping with CMR imaging.," JACC. Cardiovasc. Imaging, vol. 6, no. 7, pp. 806–22, Jul. 2013.

[4] S. Giri, Y.-C. Chung, A. Merchant, G. Mihai, S. Rajagopalan, S. V Raman, and O. P. Simonetti, "T2 quantification for improved detection of myocardial edema.," J. Cardiovasc. Magn. Reson., vol. 11, no. 1, p. 56, Jan. 2009.

[5] P. Thavendiranathan, M. Walls, S. Giri, D. Verhaert, S. Rajagopalan, S. Moore, O. P. Simonetti, and S. V Raman, "Improved detection of myocardial involvement in acute inflammatory cardiomyopathies using T2 mapping.," Circ. Cardiovasc. Imaging, vol. 5, no. 1, pp. 102–10, Jan. 2012.

[6] M. Henningsson and R. M. Botnar, "Advanced respiratory motion compensation for coronary MR angiography.," Sensors (Basel)., vol. 13, no. 6, pp. 6882–99, Jan. 2013.

[7] D. Piccini, A. Littmann, S. Nielles-Vallespin, and M. O. Zenge, "Respiratory self-navigation for whole-heart bright-blood coronary MRI: methods for robust isolation and automatic segmentation of the blood pool.," Magn. Reson. Med., vol. 68, no. 2, pp. 571–9, Aug. 2012.

[8] K. Nehrke, P. Bornert, D. Manke, and J. Bock, "Free-breathing Cardiac MR Imaging: Study of Implications of Respiratory Motion—Initial Results 1," Radiology, 2001.

[9] M. Henningsson, J. Smink, R. Razavi, and R. M. Botnar, "Prospective respiratory motion correction for coronary MR angiography using a 2D image navigator.," Magn. Reson. Med., vol. 69, no. 2, pp. 486–94, Feb. 2013.

[10] J. T. Bushberg, J. A. Seibert, E. M. Leidholdt, and J. M. Boone, The Essential Physics of Medical Imaging, 2nd ed. Philadelphia: Lippincott Williams & Wilkins, 2002.

[11] A. H. Goenka, H. Wang, and S. D. Flamm, "Cardiac magnetic resonance imaging for the investigation of cardiovascular disorders. Part 2: emerging applications.," Tex. Heart Inst. J., vol. 41, no. 2, pp. 135–43, Apr. 2014.

[12] R. C. Cury, K. Shash, J. T. Nagurney, G. Rosito, M. D. Shapiro, C. H. Nomura, S. Abbara, F. Bamberg, M. Ferencik, E. J. Schmidt, D. F. Brown, U. Hoffmann, and T. J. Brady, "Cardiac magnetic resonance with T2-weighted imaging improves detection of patients with acute coronary syndrome in the emergency department.," Circulation, vol. 118, no. 8, pp. 837–44, Aug. 2008.

[13] D. O h-Ici, J. P. Ridgway, T. Kuehne, F. Berger, S. Plein, M. Sivananthan, and D. R. Messroghli, "Cardiovascular magnetic resonance of myocardial edema using a short inversion time inversion recovery (STIR) black-blood technique: diagnostic accuracy of visual and semi-quantitative assessment.," J. Cardiovasc. Magn. Reson., vol. 14, no. 1, p. 22, Jan. 2012.

[14] O. P. Simonetti, J. P. Finn, R. D. White, G. Laub, and D. A. Henry, "'Black blood' T2-weighted inversion-recovery MR imaging of the heart.," Radiology, vol. 199, no. 1, pp. 49–57, Apr. 1996.

[15] H. Abdel-Aty, P. Boyé, A. Zagrosek, R. Wassmuth, A. Kumar, D. Messroghli, P. Bock, R. Dietz, M. G. Friedrich, and J. Schulz-Menger, "Diagnostic performance of cardiovascular magnetic resonance in patients with suspected acute myocarditis: comparison of different approaches.," J. Am. Coll. Cardiol., vol. 45, no. 11, pp. 1815–22, Jun. 2005.

[16] P. Kellman, A. H. Aletras, C. Mancini, E. R. McVeigh, and A. E. Arai, "T2-prepared SSFP improves diagnostic confidence in edema imaging in acute myocardial infarction compared to turbo spin echo.," Magn. Reson. Med., vol. 57, no. 5, pp. 891–7, May 2007.

[17] H. Ding, L. Fernandez-de-Manuel, M. Schär, K. H. Schuleri, H. Halperin, L. He, M. Muz Zviman, R. Beinart, and D. A. Herzka, "Three-dimensional whole-heart T2 mapping at 3T.," Magn. Reson. Med., Sep. 2014.

[18] R. B. van Heeswijk, D. Piccini, H. Feliciano, R. Hullin, J. Schwitter, and M. Stuber, "Self-navigated isotropic three-dimensional cardiac T2 mapping.," Magn. Reson. Med., May 2014.

[19] R. Wassmuth, M. Prothmann, W. Utz, M. Dieringer, F. von Knobelsdorff-Brenkenhoff, A. Greiser, and J. Schulz-Menger, "Variability and homogeneity of cardiovascular magnetic resonance myocardial T2-mapping in volunteers compared to patients with edema.," J. Cardiovasc. Magn. Reson., vol. 15, no. 1, p. 27, Jan. 2013.

[20] J. Xie, X. Bi, Z. Fan, H. Bhat, S. Shah, S. Zuehlsdorff, and D. Li, "3D flow-independent peripheral vessel wall imaging using T(2)-prepared phase-sensitive inversion-recovery steady-state free precession.," J. Magn. Reson. Imaging, vol. 32, no. 2, pp. 399–408, Aug. 2010.

[21] R. L. Ehman and J. P. Felmlee, "Adaptive technique for high-definition MR imaging of moving structures.," Radiology, vol. 173, no. 1, pp. 255–63, Oct. 1989.

[22] A. Scott, J. Keegan, and D. Firmin, "Beat-to-beat respiratory motion correction with near 100% efficiency: a quantitative assessment using high-resolution coronary artery imaging," Magn. Reson. Imaging, 2011.

[23] M. Henningsson, P. Koken, C. Stehning, R. Razavi, C. Prieto, and R. M. Botnar, "Whole-heart coronary MR angiography with 2D self-navigated image reconstruction," Magn. Reson. Med., vol. 67, no. 2, pp. 437–445, Feb. 2012.

[24] Y. Wang, S. J. Riederer, and R. L. Ehman, "Respiratory Motion of the Heart: Kinematics and the Implications for the Spatial Resolution in Coronary Imaging," Magn. Reson. Med., vol. 33, no. 5, pp. 713–719, May 1995.

[25] T.-Y. Huang, Y.-J. Liu, A. Stemmer, and B. P. Poncelet, "T2 measurement of the human myocardium using a T2-prepared transient-state TrueFISP sequence.," Magn. Reson. Med., vol. 57, no. 5, pp. 960–6, May 2007.

[26] U. Blume, T. Lockie, C. Stehning, S. Sinclair, S. Uribe, R. Razavi, and T. Schaeffter, "Interleaved T(1) and T(2) relaxation time mapping for cardiac applications.," J. Magn. Reson. Imaging, vol. 29, no. 2, pp. 480–7, Feb. 2009.

[27] H. Guo, W.-Y. Au, J. S. Cheung, D. Kim, J. H. Jensen, P.-L. Khong, Q. Chan, K. C. Chan, C. Tosti, H. Tang, T. R. Brown, W. W. M. Lam, S.-Y. Ha, G. M. Brittenham, and E. X. Wu, "Myocardial T2 quantitation in patients with iron overload at 3 Tesla.," J. Magn. Reson. Imaging, vol. 30, no. 2, pp. 394–400, Aug. 2009.

[28] D. Verhaert, P. Thavendiranathan, S. Giri, G. Mihai, S. Rajagopalan, O. P. Simonetti, and S. V Raman, "Direct T2 quantification of myocardial edema in acute ischemic injury.," JACC. Cardiovasc. Imaging, vol. 4, no. 3, pp. 269–78, Mar. 2011.

[29] A. A. Usman, K. Taimen, M. Wasielewski, J. McDonald, S. Shah, S. Giri, W. Cotts, E. McGee, R. Gordon, J. D. Collins, M. Markl, and J. C. Carr, "Cardiac magnetic resonance T2 mapping in the monitoring and follow-up of acute cardiac transplant rejection: a pilot study.," Circ. Cardiovasc. Imaging, vol. 5, no. 6, pp. 782–90, Nov. 2012.

[30] D. Kübler, M. Gräfe, B. Schnackenburg, C. Knosalla, K. Wassilew, J.-H. Hassel, E. Ivanitzkaja, D. Messroghli, E. Fleck, and S. Kelle, "T1 and T2 mapping for tissue characterization of cardiac myxoma.," Int. J. Cardiol., vol. 169, no. 1, pp. e17–20, Oct. 2013.

[31] E. Tunnicliffe and M. Robson, "Optimising acquisition parameters for myocardial T2 mapping using T2-prep at 3T," J. Cardiovasc. Magn. Reson., vol. 15, no. Suppl 1, p. W10, 2013.

[32] J. R. Arnold, T. D. Karamitsos, P. Bhamra-Ariza, J. M. Francis, N. Searle, M. D. Robson, R. K. Howells, R. P. Choudhury, O. E. Rimoldi, P. G. Camici, A. P. Banning, S. Neubauer, M. Jerosch-Herold, and J. B. Selvanayagam, "Myocardial oxygenation in coronary artery disease: insights from blood oxygen level-dependent magnetic resonance imaging at 3 tesla.," J. Am. Coll. Cardiol., vol. 59, no. 22, pp. 1954–64, May 2012.

[33] R. B. van Heeswijk, H. Feliciano, C. Bongard, G. Bonanno, S. Coppo, N. Lauriers, D. Locca, J. Schwitter, and M. Stuber, "Free-breathing 3 T magnetic resonance T2-mapping of the heart.," JACC. Cardiovasc. Imaging, vol. 5, no. 12, pp. 1231–9, Dec. 2012.

[34] F. von Knobelsdorff-Brenkenhoff, M. Prothmann, M. A. Dieringer, R. Wassmuth, A. Greiser, C. Schwenke, T. Niendorf, and J. Schulz-Menger, "Myocardial T1 and T2 mapping at 3 T: reference values, influencing factors and implications.," J. Cardiovasc. Magn. Reson., vol. 15, p. 53, Jan. 2013.

[35] H.-J. Yang, B. Sharif, J. Pang, A. Kali, X. Bi, I. Cokic, D. Li, and R. Dharmakumar, "Free-breathing, motion-corrected, highly efficient whole heart T2 mapping at 3T with hybrid radial-cartesian trajectory.," Magn. Reson. Med., Mar. 2015.

[36] M. E. Andia, M. Henningsson, T. Hussain, A. Phinikaridou, A. Protti, G. Greil, and R. M. Botnar, "Flow-independent 3D whole-heart vessel wall imaging using an interleaved T2-preparation acquisition.," Magn. Reson. Med., vol. 69, no. 1, pp. 150–7, Jan. 2013.

[37] K. R. Johnson, S. J. Patel, A. Whigham, A. Hakim, R. I. Pettigrew, and J. N. Oshinski, "Three-dimensional, time-resolved motion of the coronary arteries.," J. Cardiovasc. Magn. Reson., vol. 6, no. 3, pp. 663–73, Jan. 2004.

[38] A. H. Aletras, P. Kellman, J. A. Derbyshire, and A. E. Arai, "ACUT2E TSE-SSFP: a hybrid method for T2-weighted imaging of edema in the heart.," Magn. Reson. Med., vol. 59, no. 2, pp. 229–35, Feb. 2008.

[39] S. Giri, S. Shah, H. Xue, Y.-C. Chung, M. L. Pennell, J. Guehring, S. Zuehlsdorff, S. V Raman, and O. P. Simonetti, "Myocardial T_2 mapping with respiratory navigator and automatic nonrigid motion correction.," Magn. Reson. Med., vol. 68, no. 5, pp. 1570–8, Nov. 2012.

[40] W. D. Foltz, O. Al-Kwifi, M. S. Sussman, J. A. Stainsby, and G. A. Wright, "Optimized spiral imaging for measurement of myocardial T2 relaxation.," Magn. Reson. Med., vol. 49, no. 6, pp. 1089–97, Jun. 2003.

[41] C. B. Higgins, R. Herfkens, M. J. Lipton, R. Sievers, P. Sheldon, L. Kaufman, and L. E. Crooks, "Nuclear magnetic resonance imaging of acute myocardial infarction in dogs: alterations in magnetic relaxation times.," Am. J. Cardiol., vol. 52, no. 1, pp. 184–8, Jul. 1983.

[42] J. Keegan, P. D. Gatehouse, S. K. Prasad, and D. N. Firmin, "Improved turbo spin-echo imaging of the heart with motion-tracking.," J. Magn. Reson. Imaging, vol. 24, no. 3, pp. 563–70, Sep. 2006.

[43] C. B. Higgins, P. Lanzer, D. Stark, E. Botvinick, N. B. Schiller, L. Crooks, L. Kaufman, and M. J. Lipton, "Imaging by nuclear magnetic resonance in patients with chronic ischemic heart disease.," Circulation, vol. 69, no. 3, pp. 523–31, Mar. 1984.

[44] M. T. McNamara, C. B. Higgins, N. Schechtmann, E. Botvinick, M. J. Lipton, K. Chatterjee, and E. G. Amparo, "Detection and characterization of acute myocardial infarction in man with use of gated magnetic resonance.," Circulation, vol. 71, no. 4, pp. 717–24, Apr. 1985.

[45] D. S. Fieno, S. M. Shea, Y. Li, K. R. Harris, J. P. Finn, and D. Li, "Myocardial perfusion imaging based on the blood oxygen level-dependent effect using T2-prepared steady-state free-precession magnetic resonance imaging.," Circulation, vol. 110, no. 10, pp. 1284–90, Sep. 2004.

[46] A. D. Scott, J. Keegan, and D. N. Firmin, "Motion in cardiovascular MR imaging.," Radiology, vol. 250, no. 2, pp. 331–51, Feb. 2009.

[47] R. Nezafat, M. Stuber, R. Ouwerkerk, A. M. Gharib, M. Y. Desai, and R. I. Pettigrew, "B1-insensitive T2 preparation for improved coronary magnetic resonance angiography at 3 T.," Magn. Reson. Med., vol. 55, no. 4, pp. 858–64, Apr. 2006.

[48] M. G. Friedrich, H. Abdel-Aty, A. Taylor, J. Schulz-Menger, D. Messroghli, and R. Dietz, "The salvaged area at risk in reperfused acute myocardial infarction as visualized by cardiovascular magnetic resonance.," J. Am. Coll. Cardiol., vol. 51, no. 16, pp. 1581–7, Apr. 2008.

[49] J. R. MacFall, S. J. Riederer, and H. Z. Wang, "An analysis of noise propagation in computed T2, pseudodensity, and synthetic spin-echo images.," Med. Phys., vol. 13, no. 3, pp. 285–92, Jan. 1986.

[50] D. Kim, O. Gonen, N. Oesingmann, and L. Axel, "Comparison of the effectiveness of saturation pulses in the heart at 3T," Magn. Reson. Med., vol. 59, no. 1, pp. 209–215, Jan. 2008.

[51] H. K. Song and L. Dougherty, "k-space weighted image contrast (KWIC) for contrast manipulation in projection reconstruction MRI.," Magn. Reson. Med., vol. 44, no. 6, pp. 825–32, Dec. 2000.

[52] L. Feng, R. Otazo, H. Jung, J. H. Jensen, J. C. Ye, D. K. Sodickson, and D. Kim, "Accelerated cardiac T2 mapping using breath-hold multiecho fast spin-echo pulse sequence with k-t FOCUSS," Magn. Reson. Med., vol. 65, no. 6, pp. 1661–1669, Jun. 2011.

[53] M. Weiger, K. P. Pruessmann, and P. Boesiger, "2D sense for faster 3D MRI," Magma Magn. Reson. Mater. Physics, Biol. Med., vol. 14, no. 1, pp. 10–19, Feb. 2002.

[54] M. Blaimer, F. A. Breuer, M. Mueller, N. Seiberlich, D. Ebel, R. M. Heidemann, M. A. Griswold, and P. M. Jakob, "2D-GRAPPA-operator for faster 3D parallel MRI.," Magn. Reson. Med., vol. 56, no. 6, pp. 1359–64, Dec. 2006.

[55] M. Doneva, P. Börnert, H. Eggers, C. Stehning, J. Sénégas, and A. Mertins, "Compressed sensing reconstruction for magnetic resonance parameter mapping.," Magn. Reson. Med., vol. 64, no. 4, pp. 1114–20, Oct. 2010.

[56] C. Huang, C. G. Graff, E. W. Clarkson, A. Bilgin, and M. I. Altbach, "T2 mapping from highly undersampled data by reconstruction of principal component coefficient maps using compressed sensing.," Magn. Reson. Med., vol. 67, no. 5, pp. 1355–66, May 2012.